Anexo B: publicación complementaria O1-2C

En este anexo se presenta la publicación complementaria O1-2C, ver Figura 12 y Sección 5.2.4.2 en Capítulo 5. En el siguiente cuadro se resumen el título del trabajo, los autores, el nombre de la revista, su clasificación en JCR y Scopus, y su ISSN. Además, se agrega información general del artículo, como el volumen y número, si es o no de acceso abierto, el año y rango de páginas, el DOI, las palabras clave y el resumen en inglés.

Publicación	O1-2C	
Título	A Finite Element Analysis and an Improved Induced Charge Concept for Partial Discharge Modeling	
Autores	Moein Borghei, Mona Ghassemi, Johnatan M. Rodríguez-Serna y Ricardo Albarracín-Sánchez	
Universidades colaboradoras	Universidad Politécnica de Madrid, Universidad de Antioquia (Colombia), Virginia Tech. (Estados Unidos de América)	
Revista	IEEE Transactions on Power Delivery	
Clasificación	JCR: Q1, Scopus: Q1.	
ISSN	0885-8977	
Volumen (número)	- (-), aceptado, disponible en modo "*early access*"	
Año, páginas	2020, 11	
DOI	**https://doi.org/10.1109/TPWRD.2020.2991589**	
Publicación de acceso abierto	Sí	
	No	X
Keywords	Finite element analysis, induced charge concept, partial discharge modelling.	
Abstract	Although much work has been done and significant progress has been made on partial discharges (PD) measurement and detection techniques, this is not the case for PD modelling. Four types of internal PD modelling, in sequential order from first to last developed, are three-capacitance (abc), induced charge concept (ICC), finite element analysis (FEA), and Multiphysics models. The abc model is too simple to provide an understanding of the physical phenomena affecting PD. In contrast, Multiphysics models are immature. Multiphysics models require a high number of physical parameters that need to be experimentally determined, which not a trivial task is. Moreover, adjusting the physical parameters to achieve a good agreement between simulation results and measurement results for a specific geometry and dimension may not work for other geometries and dimensions. The FEA model, a relatively recent model, and the ICC model, which fall between the abc and Multiphysics models in terms of modelling complexity, can partly explain mechanisms and physical phenomena associated with internal PD. However, to the best of our knowledge, there is only one paper comparing ICC and FEA models for a case study; thus, further research is needed to elucidate various aspects of these two models. In this paper, 1) an improved ICC and a FEA capable of describing phenomena occurring during PD are developed, 2) both developed models are coded and implemented either in MATLAB® or in COMSOL Multiphysics® linked with MATLAB®, and their simulation results are compared and analysed, and 3) the influence of different parameters including void shape, void size, and void air pressure on PD parameters are studied.	

A Finite Element Analysis and an Improved Induced Charge Concept for Partial Discharge Modeling

Moein Borghei, *Student Member, IEEE*, Mona Ghassemi, *Senior Member, IEEE*,
Johnatan M. Rodríguez-Serna and Ricardo Albarracín-Sánchez

***Abstract*—Although much work has been done and significant progress has been made on partial discharges (PD) measurement and detection techniques, this is not the case for PD modeling. Four types of internal PD modeling, in sequential order from first to last developed, are three-capacitance (abc), induced charge concept (ICC), finite element analysis (FEA), and Multiphysics models. The abc model is too simple to provide an understanding of the physical phenomena affecting PD. In contrast, Multiphysics models are immature. Multiphysics models require a high number of physical parameters that need to be experimentally determined, which is not a trivial task. Moreover, adjusting the physical parameters to achieve a good agreement between simulation results and measurement results for a specific geometry and dimension may not work for other geometries and dimensions. The FEA model, a relatively recent model, and the ICC model, which fall between the abc and Multiphysics models in terms of modeling complexity, can partly explain mechanisms and physical phenomena associated with internal PD. However, to the best of our knowledge, there is only one paper comparing ICC and FEA models for a case study; thus, further research is needed to elucidate various aspects of these two models. In this paper, 1) an improved ICC and a FEA capable of describing phenomena occurring during PD are developed, 2) both developed models are coded and implemented either in MATLAB or in COMSOL Multiphysics linked with MATLAB, and their simulation results are compared and analyzed, and 3) the influence of different parameters including void shape, void size, and void air pressure on PD parameters are studied.**

***Index Terms*—Finite element analysis, induced charge concept, partial discharge modeling.**

I. Introduction

ACCORDING to IEC 60270, partial discharges (PD) are localized electrical discharges that only partially bridge the insulation between conductors and may or may not occur adjacent to a conductor. PD have the largest effect on insulation degradation [1].

Electrical insulation status often determines the lifespan of power system apparatuses. Replacement of a faulted power system component can take up to a few days, and during that contingency time, the power grid is more prone to blackouts. Thus, condition and health monitoring of electrical assets for planned replacements where single contingency time can be minimized is highly needed for resiliency enhancement of current and future modern power grids. Actions for resiliency enhancement of power grids consist of corrective actions and preventive actions. Corrective actions such as load shedding and/or network reconfiguration are done during and after the occurrence of a disaster. Preventive actions such as line undergrounding, elevating substations, and vegetation management, and condition monitoring discussed above result in hardening the system infrastructure and, in turn, its resiliency enhancement. One of the critical parameters for condition monitoring and health assessment of power system apparatuses is the online monitoring of their PD activities and history. Understanding the mechanisms and phenomena affecting PD through modeling plays a critical role in the interpretation and development of health indexes based on PD measurements.

Although PD detection and localization techniques have matured [2-6], to cite a few, this is not the case for PD modeling. To date, four types of PD modeling for a void-solid dielectric system have been proposed.

The abc model initiated by Whitehead presents an equivalent circuit, including three capacitances, to model the void inside an insulating material [7]. Although it is a simple model, it provides appropriate insight into PD phenomena from a macroscopic standpoint. However, the model does not (and cannot) truly represent the physical processes that occur within a real system [8]. On the other hand, although Multiphysics models [9, 10] may be able to accurately model mechanisms and phenomena associated with PD, there are many physical parameters in the model that need to be experimentally determined.

In this paper, an improved ICC and a FEA capable of describing phenomena occurring during PD are developed. To the best of our knowledge, ICC and FEA models have been compared for a case study in only one paper [11]. Also, although models for internal PD in solid dielectrics have recently been reviewed in [12], simulation results presented in the paper are from different case studies (not for just one case study) studied in the literature. In other words, since case studies are different in terms of geometry, dimension, type, and magnitude of applied voltage, their results cannot be compared together. This issue is addressed in this paper.

Both ICC and FEA models are delineated and implemented, respectively, in Section II and Section III. The phase-resolved PD (PRPD) patterns are obtained through both models. Simulation results obtained from two methods for the same case study are compared and discussed in Section IV. Moreover, the influence of different geometrical parameters of a void within a solid dielectric as well as its air pressure on PD parameters are

M. Borghei and M. Ghassemi are with the ECE Dept., Virginia Tech, Blacksburg, VA 24061 USA (e-mails: {moeinrb, monag}@vt.edu).

J. M. Rodríguez-Serna and R. Albarracín-Sánchez are with the Escuela Técnica Superior de Ingeniería y Diseño Industrial (ETSIDI)-Universidad Politécnica de Madrid (UPM), Electrical and Electronic Engineering, Automatic Control, Applied Physics Department, Ronda de Valencia 3, Madrid 28012, Spain (e-mails: johnatan.rodriguez.serna@alumnos.upm.es, ricardo.albarracin@upm.es).

J. M. Rodríguez-Serna is also with the Electrical Engineering Dept., Universidad de Antioquia, Calle 67 No. 53–108, Medellín, Colombia.

analyzed in Section V. Finally, the conclusions to the work are presented in Section VI.

II. FEA Model Development

A. Streamer Inception Criterion

A PD event in a gas-filled void located in a solid dielectric can be launched right after the free electrons gain enough energy to be accelerated, ionize further molecules and atoms due to impact ionization, and eventually lead to streamer formation. In this regard, the minimum electric field intensity inside the void at which the discharge path can reach its maximum length is known as the inception electric field (E_{inc}). The maximum length is the scale of the void parallel to the electric field direction along which the discharge can propagate. The streamer breakdown criterion, E_{inc} for an ellipsoidal void can be given by [8]:

For an electron attaching gas (such as SF_6):

$$E_{\text{inc}}/p = (1 + M/2ap)(E/p)_{cr} \tag{1}$$

For a non-attaching gas (such as air):

$$E_{\text{inc}}/p = (1 + B/(2ap)^n)(E/p)_{cr} \tag{2}$$

where p is gas pressure and a is the radius of the ellipsoidal void parallel to the background field. n, B, and $(E/p)_{cr}$ are gas-related parameters for the ionization process. M is the figure of merit for the attaching gas and is defined in [8] as a function of $(E/p)_{cr}$.

B. Initial Electron Generation

Another condition for PD occurrence is that the existence of initial electrons for the ionization process must be ensured. One should characterize two different concepts of electron production. One is the initial electron generation described in this section, and another is the electron avalanche resulted, for example, by the collisions among the accelerated electrons and atoms/molecules.

B.1 A Theoretical-based Formulation

There are two processes, volume ionization, and surface emission, for the generation of initial electrons in the void. Each includes the following mechanisms [13].

Surface Emission:
- I. Detrapping of electrons from the surface of the insulator
- II. Electron emission by photo effect from the surface of the insulator
- III. Unleashing electrons by ion impact
- IV. Electron emission by photo effect from the surface of the conductor
- V. Electron release from the conductor due to the electric field

Volume Ionization:
- VI. Gas ionization by irradiation of energetic photons
- VII. Detachment of electrons from negative ions due to field intensity

Thus, the total rate of the generation of initial electrons per unit of time can be expressed as the summation of the electron generation rates due to each of the processes:

$$\dot{N_{tot}}(t) = \dot{N_{surf}}(t) + \dot{N_{vol}}(t) \tag{3}$$

where $\dot{N_{surf}}(t)$ is the electron generation rate due to surface emission and $\dot{N_{vol}}(t)$ quantifies the contribution of the volume ionization. In the following parts, each of these processes is delineated in detail.

B.1.1 Surface Emission

In surface emission, electrons are emitted from the void surface by mechanisms I through V mentioned in Section B.1. The dominating mechanism of surface emission is the detrapping of electrons accumulated on the surface of the void [14], which is dependent upon the electric field and the temperature inside the void. Thus, the electron generation rate due to the surface emission process ($\dot{N_{e,surf}}$) can be fitted to Richardson-Schottky scaling given by [13-15]:

$$\dot{N_{e,surf}} = N_{e,surf}\nu_0 \exp\left(-\left(\phi - \sqrt{eE_{cav}/4\pi\varepsilon_0}\right)/kT\right) \tag{4}$$

where $\nu_0 \approx 10^{13} - 10^{14}\ \text{s}^{-1}$ [13] is the fundamental phonon frequency of the material (for epoxy resin $\nu_0 \approx 10^{14}\ \text{s}^{-1}$ [15]). The effective detrapping work function of the material, ϕ, is in eV units, and e is the elementary charge of the electron. The surface emission rate can sensitively change with respect to the value of ϕ [13]. The effective detrapping work function integrally takes into account all the properties of the void surface related to surface emission like material, microroughness, and chemical state [15]. The emission current density is highly sensitive to the exact value of ϕ which varies between $1 - 1.3\ eV$ [13]. In order to select the proper value, this parameter should be calibrated to the experimental results. E_{cav} is the electric field intensity inside the void due to surface charges on the void wall, $\varepsilon_0 = 8.854 \times 10^{-12}\ \text{F.m}^{-1}$ is the vacuum permittivity, $k = 8.6174 \times 10^{-5}\ \text{eV.K}^{-1}$ is Boltzmann's constant, and T is the absolute temperature. $N_{e,surf}$ is the number of electrons available to be detrapped from the void surface for the next PD. In [14] it was assumed that the total true physical charge of the previous PD, q, can participate in the detrapping mechanism and, thus, $N_{e,surf}$ was approximated by q/e. However, it was assumed in [13, 15] that this number is affected by two factors delineated below. The first factor, known as the proportionality factor ($\xi < 1$), describes the fraction of the charge carriers that result in the creation of detrappable electrons. The contribution of this factor denoted as $N_{e,surf0}$ is given by

$$N_{e,surf0} = \xi(q/e) \tag{5}$$

In Fig. 1, the movement of charged particles is shown under two different conditions. The electric field due to the applied voltage ($E_{app}(t)$) is one of two components of the electric field inside the void. However, owing to the lower permittivity of the gas inside the void than that of the solid dielectric, the magnitude of $E_{app}(t)$ is multiplied by an enhancement factor (f) that quantifies the intensification of $E_{app}(t)$ inside the void. The derivation of f will be discussed later in (17). Aside from

$fE_{app}(t)$, the electric field inside the void includes another component, called $E_{int}(t)$, which is the electric field due to surface charges remaining on the surface of the void from the previous PD events. The summation of these two components yields the net electric field magnitude inside the void ($E_{cav}(t)$).

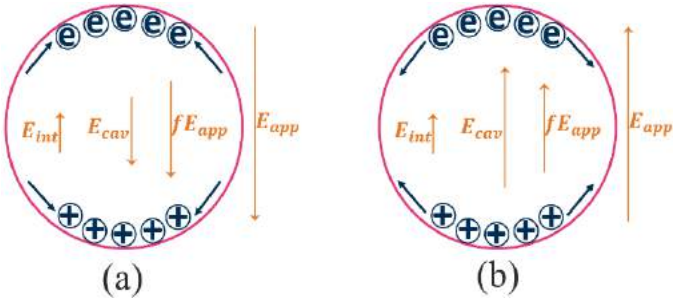

Fig. 1. The demonstration of the movement of charged particles in the void when the direction of electric field between two consecutive PD (a) does not change, (b) changes.

In Fig. 1a, the direction of $E_{app}(t)$ remains constant between two consecutive PD and the charged particles move in the opposite direction. On the other hand, when the direction of $E_{app}(t)$ changes between two consecutive PD events, the directions of the two field components would be the same. Thus, the positive ions and electrons approach each other (Fig. 1b). Due to the neutralization of the charged particles, the number of available electrons for the upcoming PD event is reduced. Therefore, a global value for the proportionality factor (ξ) may not provide an accurate explanation for the estimation. When the polarity of electric field changes between two consecutive events, the electron detrapping mechanism is much more difficult from a negatively charged void surface than the case of a positively charged one. To distinguish these two scenarios, ξ_+ and ξ_- are defined for positively and negatively charged void surfaces, respectively.

As the second factor, while $N_{e,surf0}$ electrons are expected to accumulate on the void wall, it is also expected that these electrons decay during the time intervals between events. The decay processes may cause the electrons in the shallow traps to hop into deeper ones, from which it is very hard to be detrapped. The electrons might also become inactive in PD ignition by diffusing into the depth of insulating medium [13, 14]. Considering the influence of the two factors, $N_{e,surf}$ is given by [13-15]

$$N_{e,surf} = N_{e,surf0} \exp\left(-t/\tau_{decay}\right) \tag{6}$$

where t is the time passed from the last PD event and τ_{decay} is the decay effective time constant.

B.1.2 Volume Ionization

While some studies have neglected the contribution of volume ionization owing to a lower rate of electron generation compared to surface emission [7, 14, 15], volume ionization is the dominant provider of free electrons in some cases. There might be some times at which free electrons cannot be supplied from surface emission mechanisms such as is the case of the first PD event. At the first PD event, no electron is available to be detrapped from the void wall; thus, volume ionization plays a significant role. As the rate of electron generation due to volume ionization is much lower than the surface emission, there is a considerable inception delay time before the occurrence of the first PD. Volume ionization might occur due to the irradiation of energetic photons (mechanism VI) or field detachment of electrons from negative ions (mechanism VII) [13]. The electron generation rate due to volume ionization ($\dot{N_{e,vol}}$) is dominated by irradiation of energetic photons and can be calculated as [13, 14]:

$$\dot{N_{e,vol}} = C_{rad}\Phi_{rad}\,(\rho/p)_0\,p\,V_{eff} \tag{7}$$

where C_{rad} is a parameter for modeling the interaction between gas molecules and radiation, Φ_{rad} is the quantum flux density of the radiation (at atmospheric pressure: $C_{rad}\Phi_{rad} = 2\times 10^6\ \mathrm{kg^{-1}s^{-1}}$). $(\rho/p)_0 = 10^{-5}\ \mathrm{kg.m^{-3}.Pa^{-1}}$ is the pressure reduced density of the gas. The term V_{eff} stands for the void volume. For an ellipsoidal void, it equals $4\pi abc/3$ where a, b, and c are the axes of the ellipsoidal void. In [13], another term called the Legler function, $(1-\eta/\alpha)$, multiplies the right-hand side of (7); it considers the probability that the electron can lead to an electron avalanche. The parameters η and α stand for the gas attachment coefficient and the gas ionization coefficient, respectively. In the PD phenomenon, usually $\eta \ll \alpha$, which makes the Legler function close to unity. As the whole electron generation rate will later be employed to find the probability of PD occurrence, it would be unnecessary to involve the Legler function to evaluate the probability of avalanche ignition.

B.2 An Experimental-based Formulation

As the theoretical-based formulations of electron generation processes discussed in Section B.1 require some physical parameters that are not widely available, a somewhat simplified model has been introduced in [16-20] based on adjustment of the experimental results. By neglecting the contribution of volume ionization, the electron generation rate ($\dot{N_{tot}}(t)$) was modeled as [17]

$$\dot{N_{tot}}(t) = N_{es}\exp(|U_{cav}(t)/U_{\mathrm{inc}}|) \tag{8}$$

where N_{es} is a constant, $U_{cav}(t)$ is the voltage of the void center, and U_{inc} is the inception voltage for discharge. A more sophisticated model taking both electron generation processes into account was proposed in [16, 18-20]:

$$\dot{N_{tot}}(t) = \dot{N_{surf}}(t) + N_{vol} \tag{9}$$

where N_{vol} is a constant representing the contribution of volume ionization. The electron generation rate due to surface emission ($\dot{N_{surf}}(t)$) is assumed to be proportional to the PD charge magnitude of previous events since they are the resources of trapped electrons at the void surface. Thus, $\dot{N_{surf}}(t)$ can be calculated by [16]:

$$\dot{N_{surf}}(t) = N_{PD}\exp(|E_{cav}(t)/E_{\mathrm{inc}}|)\exp\left(-(t-t_{PD})/\tau_{decay}\right) \tag{10}$$

where the first exponential term considers the effect of the electric field, and the second one represents the decay of PD charges by time after its occurrence at t_{PD}. The PD charge magnitude is modeled as [16]:

$$N_{PD} = N_{es0}\,|E_{cav}(t_{PD})/E_{\mathrm{inc}}| \tag{11}$$

where N_{es0} is assumed to be the incipient number of electrons at the time that electric field inside the void reaches the inception field $E_{\rm inc}$. The constants N_{vol}, N_{es0}, and τ_{decay} are determined in a way to have an acceptable level of agreement with experimental results.

C. Surface Charge Decay

As mentioned earlier, the amount of charges accumulated on the void surface varies over time; during electron avalanche, the number of electrons increases, and these generated electrons will decay between PD events. In section B.1, it was discussed how to take into account the impact of surface charge decay on the electron generation rate. However, in the FEA model, the contribution of surface charge decay should also be involved in the dynamic modeling of PD. The trapped charges can hop into deeper traps, which makes it harder to detrap electrons for PD ignition, yet they take part in the potential difference across the void [16]. Electrons may also decay through diffusing into the depth of the insulating material [15], which can affect the charge density on the void surface. To model the decay rate, surface conductivity can be adjusted. In [17], a charge-dependent model is proposed for surface conductivity. The surface conductivity is assigned an initial value ($\sigma_{surf,L}$). Once the electric charge on the void surface exceeds a critical amount (q_{cr}), the surface conductivity will be enhanced to a higher value ($\sigma_{surf,H}$). If the charge magnitude falls below q_{cr} again, the surface conductivity will be re-assigned its initial value ($\sigma_{surf,L}$). In [16], a field-dependent surface conductivity formula was introduced. Surface conductivity ($\sigma_s(t)$) increases from its initial value (σ_{s0}) to a higher value, which is given by a field-dependent formulation [16]:

$$\sigma_s(t) = \sigma_{s0} \exp(\alpha |E_{cav}(t)|) \tag{12}$$

where α is the stress coefficient. In [16], a maximum value of σ_s estimated through the experimental data and given by (13) was used to avoid convergence problems.

$$\sigma_{smax} = \gamma \exp(\beta\, |E_{app}(t)|) \tag{13}$$

where γ and β were experimentally determined. However, a prerequisite for using the above formula is to ensure the existence of free surface charges at the void surface. Charges at the void surface are grouped into two types: the first group consists of the trapped charges at the void surface, which was discussed before, and the other type includes free charges in the same area. The free charges can be approximated by the integration of field displacement over the upper or lower void surface (S_{void}) as:

$$q_{free}(t) = \int_{S_{void}} D(t)\,.\,dS \tag{14}$$

Then, the magnitude of the electric field due to this second group of charges ($E_{s,free}(t)$) can be calculated by:

$$E_{s,free}(t) = \left| q_{free}(t) E_{int}(t) / q_{PD,total}(t) \right| \tag{15}$$

where $q_{PD,total}$ is the total amount of true charge originating from the PD events that happened so far. Seen in Fig. 1, the electric field inside the void ($E_{cav}(t)$) consists of two components: (1) the electric field due to the applied voltage ($fE_{app}(t)$), and (2) the electric field due to the surface charges ($E_{int}(t)$). Therefore, the electric field due to surface charges can be obtained as follows:

$$E_{int}(t) = E_{cav}(t) - fE_{app}(t) \tag{16}$$

where f is the enhancement factor, which takes into account the impact of void existence on the increase in the electric field magnitude at the location of the void. In other words, fE_{app} is the electric field at the location of the void in the absence of surface charges. f can be obtained from the following equation [15].

$$f = K\varepsilon_r / 1 + (K-1)\varepsilon_r \tag{17}$$

where K is a geometrical parameter given by [13]:

$$K = \begin{cases} \sim 1 & a/b \ll 1 \\ 3 & a/b = 1 \\ \sim 4a/b & 1 < a/b < 10 \end{cases} \tag{18}$$

where a and b are the ellipsoid axes parallel and perpendicular, respectively, to the background field.

D. Modeling of the PD Process

The final step in the assessment of free electron availability is to address the stochastic nature of the phenomena. To this end, the probability of the existence of a free electron for PD ignition, $P(t)$, at each time step can be obtained [17]:

$$P(t) = 1 - \int_{t_{PD}}^{t_{PD}+t} \dot{N_{tot}}(\tilde{t}).\,d\tilde{t} \tag{19}$$

In this paper, equations (3)-(7) are used to determine $\dot{N_{tot}}$. Once the value of $P(t)$ is determined, a random number R between zero and unity is generated. If $P > R$, then PD happens; otherwise, another time step is added to the delay time for the next PD ignition. When the requirements for a PD event are satisfied, in the FEA model, the discharge is modeled as an increase in the conductivity of the void from an initial value ($\sigma_{void,0}$) to a maximum level ($\sigma_{void,max}$). The increase in the void conductivity causes a voltage drop across the void as well as a field reduction inside the void. $\sigma_{void,max}$ is a macroscopic parameter, and its role being to take into account all microscopic gas discharge processes taking place during the bridging of the cavity and inducing charged particles on the cavity wall as well as electrode surface. To achieve the above goals, $\sigma_{void,max}$ should be calibrated with the experimental results to enable the proper representation of microscopic events.

The discharge continues until a certain value of the electric field at which the ionization cannot go any further. After the extinction of PD, the conductivity of the void is returned to its initial value (σ_{s0}). However, the charges deposited on the void wall can help to accelerate the happening of the next PD event. On the other hand, in the ICC method, the PD process is modeled as an instantaneous change in the electric field strength magnitude inside the void, considering the resultant electric field inside the void is quenched by the electric field produced by surface charges left by PD. With the aid of FEA, the electrical parameters, such as field displacement and current density over different parts of the system, can be accessed. This helps to dynamically examine the changes in the electrical

characteristics of PD phenomena before, during, and after its occurrence. Thanks to the privilege of FEA, the magnitude of true and apparent charges related to each PD event can be obtained through the time integration of the current flowing through the void surface and electrode, respectively during a PD event given by

$$q_{true} = \int_{t_{inc}}^{t_{ext}} \left(\int_{S_{cav}} \vec{J}(t).d\vec{S} \right) dt \tag{20}$$

$$q_{app} = \int_{t_{inc}}^{t_{ext}} \left(\int_{S_{Electr}} \vec{J}(t).d\vec{S} \right) dt \tag{21}$$

In the above equations, $\vec{J}(t)$ is the current density over either the void surface in (20) or the electrode in (21). For the calculation of true apparent charge, the current over the upper half-area of the void is integrated between the inception and extinction time. A similar procedure is repeated for the apparent charge; however, in this case, the current over the ground electrode is used for derivation of charge magnitude.

III. ICC METHOD

After a PD event, the electric charge in the dielectric bulk and voids will induce a proportional charge on the high voltage (HV) electrode (q') that can be expressed by [21].

$$q' = -\int_{\Omega} \lambda \rho d\Omega - \sum_{j=1}^{N} \int_{S_j} \lambda \sigma dS \tag{22}$$

where Ω is the volume of the entire dielectric system, λ defined in (22) is a proportionality positive scalar function which is continuous and dimensionless, N is the number of voids, S_j is the surface of the j-th void, ρ is the volume charge density and σ is the surface charge density. According to the superposition and Green's reciprocation theorems, λ is the electric scalar potential in the dielectric system without free charges with an applied voltage of magnitude equal to 1 V. Therefore, λ satisfies (23).

$$\nabla \cdot (\varepsilon \nabla \lambda) = 0 \tag{23}$$

In addition, λ must fulfill the following boundary conditions [8]:

$$\left.\begin{array}{rr} \lambda = 1 & \text{at HV electrode} \\ \lambda = 0 & \text{at ground electrode} \\ \varepsilon_r \dfrac{\partial \lambda_m}{\partial n} = \dfrac{\partial \lambda_V}{\partial n} & \text{at interface} \end{array}\right\} \tag{24}$$

where λ_m and λ_V are the solutions at the interface location for the solid dielectric and void sides, respectively, and n is the normal direction to the interface. The charges generated during a PD event are separated and deposited on the void surface, which can be represented by a dipole, as shown in Fig. 2a where s is the vector separating the charges with opposite polarity. The dipole moment (p) of the charges on the void surface is given by [21]

$$p = \int_{\Omega} \rho r d\Omega + \int_{S} \sigma r dS \tag{25}$$

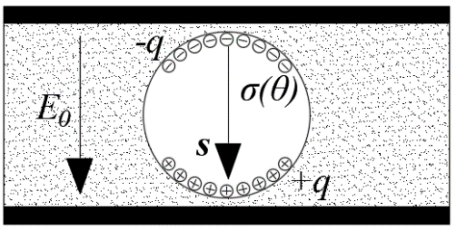

(a)

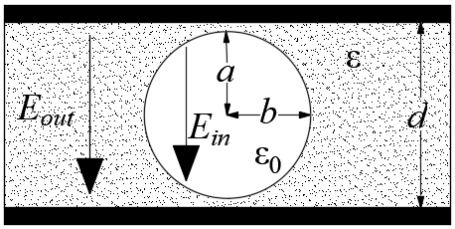

(b)

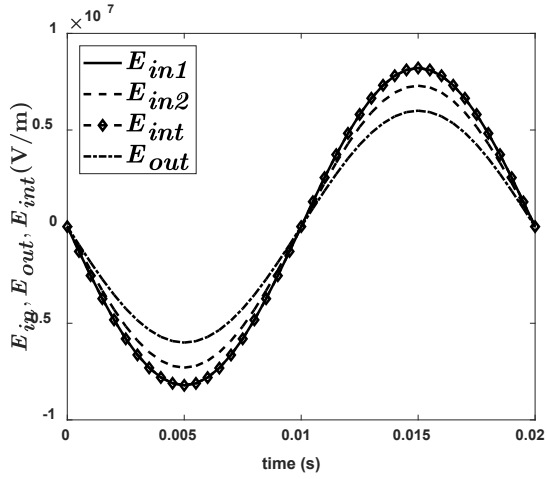

(c)

Fig. 2. a) The dipole formed due to the charges on the void surface, b) the geometry considered for obtaining f^*, c) E_{in} and E_{out} for the geometry shown in a) (E_{in1} and E_{in2} are for $a = b = 0.125$ and 1.25 mm, respectively.

where r is the position vector of the charge element. Considering that the void is small in comparison with the bulk solid dielectric size, the gradient of λ can be assumed to be uniform inside the void, and q' due to the dipole is given by

$$q' = -p \cdot \nabla \lambda \tag{26}$$

where $\nabla\lambda$ can be calculated as $\nabla\lambda = f\nabla\lambda_0$, λ_0 is the electric scalar potential at the void center location for the condition of a dielectric system without voids and charges, and f is the enhancement factor given by (17). $\nabla\lambda_0$ depends on the geometrical parameters of electrodes and homogeneous dielectric bulk. For the three most used configurations, $|\nabla\lambda_0|$ can be calculated as [22]:

$$\left.\begin{array}{rr} 1/d & \text{for plane electrodes} \\ 1/r\ln(r_{out}/r_{in}) & \text{for coaxial cylinders} \\ r_{in}r_{out}/r^2(r_{out}-r_{in}) & \text{for concentric spheres} \end{array}\right\} \tag{27}$$

where d is the distance between the HV and ground electrodes, r is the distance from the axis or point of symmetry to the void center, and r_{in} and r_{out} are the inner and outer radii of electrodes, respectively. For ellipsoidal voids, (26) will be [8]

$$q' = -K\Omega\varepsilon(E_{\text{cavPD}} - E_{\text{res}}) \cdot \nabla\lambda_0 \quad (28)$$

where K can be obtained from (18), ε is the solid dielectric permittivity, and E_{cavPD} is the electric field intensity in the void just before the PD event. E_{res} is the electric field intensity below which there is no ionization and can be calculated by [13]

$$E_{\text{res}} = \gamma(E/p)_{cr}p \quad (29)$$

where γ is a dimensionless factor depending on the polarity of streamers and is assumed as $\gamma = 0.35$ for averaging positive and negative streamers [15]. The real PD charge magnitude and the electric field intensity due to the void surface charge can be calculated by (30) and (31), respectively [13].

$$q = \varepsilon_0\pi b^2[1 + \varepsilon_r(K-1)](E_{\text{cavPD}} - E_{\text{res}}) \quad (30)$$

$$E_q(t) = q(t)/\varepsilon_0\pi b^2[1 + \varepsilon_r(K-1)] \quad (31)$$

The dipole moment approach described above and an energy balance approach, in which the field energy transferred to electrons and positive ions are equalized to the energy supplied to the void during the PD event, were used in [23] to estimate the PD charge and obtain the following expression for the induced charge.

$$q' = p \cdot \frac{E_{\text{inc}}}{U_{\text{inc}}} \quad (32)$$

Equations (26) and (32) are equivalent for a void without previous PD and neglecting the time lag, since $\nabla\lambda = E_{\text{inc}}/U_{\text{inc}}$ under the above conditions.

Moreover, the formulation through the energy balance infers that the insulation deterioration due to PD events is mainly governed by the field energy transferred to charge carriers. Note, the energy supplied to electrons and ions will produce ion bombardment, molecule excitation, and changes in temperature and pressure inside the void, leading to local erosion and eventually dielectric breakdown [24]. For this reason, it is reasonable to use this approach instead of the apparent charge concept used in the abc models.

It is difficult to obtain high precision in the dipole moment quantification in (32) because an accurate determination of the number of ionized molecules is required. However, if streamer discharges are considered, the magnitude of the dipole moment ($|p|$) in pC·mm can be calculated by the semi-empirical expression given in (33) [25]. It is considered that during the time in which the PD event elapses, the Laplacian field remains constant [25].

$$|p| = 270d_c^2 \quad (33)$$

where d_c is the void diameter in mm. This expression derived from measurements and theoretical analysis is applicable for spherical virgin voids in the range of 0.1 mm $< d_c <$ 2 mm. For virgin voids, it is assumed that the electric field inside the void is only due to an externally applied voltage and there is no electric field due to electric charges on the void surface.

Using the ICC method for simulating the PD activity in spherical cavities at five different aging phases in [15], it was found that the surface conductivity plays an important role in simulation results for aged voids. The influence of working temperature on PD behavior was studied in [14] and it was found that the void surface conductivity proportionally increases with temperature. Taking this point into account, simulation results using the ICC method showed that at a temperature higher than ambient a higher discharge time lag results, which produces a substantial decrease in the PD rate and a higher spread between minimum and maximum PD charge magnitudes.

The applicability of the ICC model is restricted to the fulfillment of the following considerations:

- The electric field intensity inside the void is uniform.
- The electric field intensity in the bulk of the solid dielectric remains unaltered during the PD event.
- The entire void volume is affected by a PD event. Note, in practice, only the volume close to the streamer channel (and not the whole void volume) is affected.

The enhancement factor (f) in (17) is independent of the solid dielectric thickness. However, as shown below, it depends on the relative dimension of the void regarding the solid dielectric thickness.

For the geometry shown in Fig. 2b, Fig. 2c shows E_{in} and E_{out} for two void radii of $a = b = 0.125$ and 1.25 mm. E_{in} is the uniform electric field intensity inside the void, and E_{out} is the electric field intensity in the bulk of the solid dielectric. The E_{in} shown in Fig. 2c was obtained by modeling the geometry shown in Fig. 2b in COMSOL Multiphysics for d=3 mm and assuming the solid dielectric as epoxy resin with $\varepsilon_r = 5.2$. The applied voltage is 50 Hz, 18 kV sinusoidal voltage, thus, $E_{out} = 6$ kV/mm. For $a = 0.125$ mm, E_{int} in Fig. 2c is the electric field intensity inside the void calculated by $E_{in} = fE_{out}$, where f is theoretically obtained from (17) and (18). As seen in Fig. 2c, E_{int} is equal to E_{in1}. However, for larger values of a as shown in Fig. 3a, E_{int} is greater than that obtained by numerical simulations. Using a numerical fitting process for the values shown in Fig. 3a, $f_{\text{mod}} = -1.271(a/d)^{2.74} + 1$ can be used as a multiplier to f obtained from (17). Thus,

$$E_{in} = f^*E_{out} \quad (34)$$

where $f^* = f_{\text{mod}} \cdot f$. With this factor, the electric field intensity inside the void is corrected from the theoretical value calculated using (17) when the void size is on the order of the dielectric bulk thickness.

The value of the electric field inside the void controls the repetition rate, the time lag, and the PD charge magnitude. On the other hand, PD events leave electric charges on the void surface that are redistributed and neutralized by surface currents. Therefore, as discussed before, the electric field intensity inside a void varies as a function of the external applied electric field and the decay of electric charges on the void surface over time.

Fig. 3b shows the behavior of surface charge density distribution on the void surface as a function of time for the geometry shown in Fig. 2b. In Fig. 3b, $\tau = \varepsilon_0 a/k_s$ where k_s is the conductivity of the void surface, $\sigma_0 = q/4\pi a^2$ where q is the real PD charge. As seen in Fig. 3b, the density of charge is symmetrically distributed on the void surface around the axis of symmetry and has a time constant that is mainly dependent on the relative permittivity. On the other hand, the surface charge is not uniformly distributed as it is assumed in the ICC method.

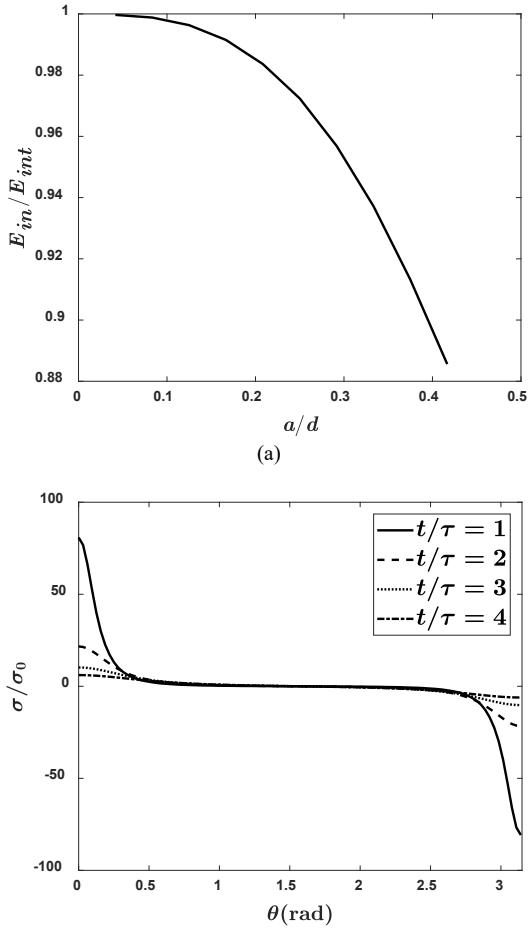

Fig. 3. a) Relation between E_{in} and E_{int} as a function of a/d, b) surface charge density distribution as a function of time for $\varepsilon_r = 5.2$, $k_s = 1 \times 10^{-18}$ S/m, $a = 0.7$ mm and $q = 674$ pC (minimal theoretical PD charge magnitude [15]).

Fig. 4a shows E_{in} along the symmetry axis at a specific instance ($t/\tau = 3$) as a function of permittivity where $E_0 = q/4\pi\varepsilon_0 a^2$ V/m. Fig. 4b shows E_{in} along the z-axis as a function of time for $\varepsilon_r = 5.2$. As seen in Figs. 4a and 4b, after a PD event, E_{in} is not uniform and its distribution depends on the charge decay process. Moreover, the electric field outside the void is also affected by the charge distribution on the void surface and should be considered since it affects the polarization process in the bulk solid dielectric.

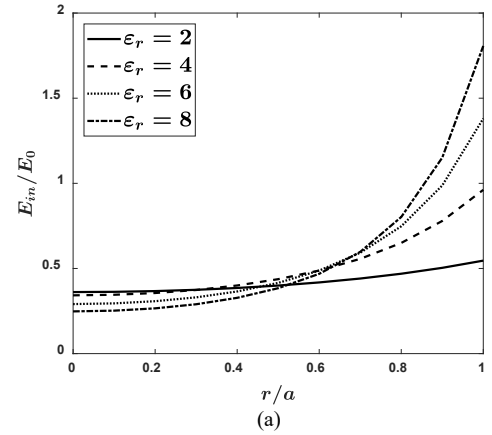

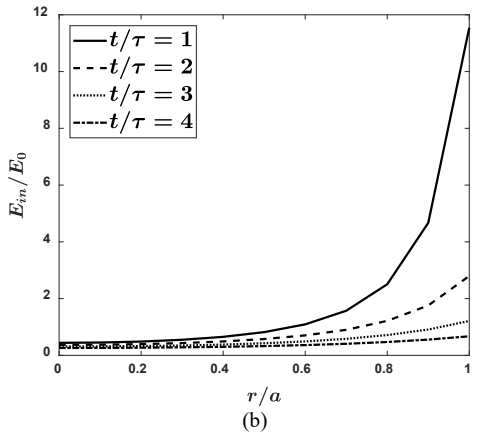

Fig. 4. a) E_{in} for different permittivity at $t/\tau = 3$, $k_s = 1 \times 10^{-18}$ s/m, r is the radial coordinate with $\theta = 0°$, $q = 674$ pC and $a = 0.7$ mm, b) E_{in} as a function of time for $\varepsilon_r = 5.2$, $k_s = 1 \times 10^{-18}$ s/m, r is the radial coordinate with $\theta = 0°$, $q = 674$ pC and $a = 0.7$ mm.

IV. Comparison Between FEA and ICC

The geometry used in simulations for comparison between the FEA and ICC methods is a cylindrical block of epoxy resin with $\varepsilon_r = 5.2$ having a radius and height of 5 and 3 mm, respectively. There is an air-filled void with a radius and thickness of 0.6 and 0.05 mm, respectively, at the center of the solid dielectric. Considering $p = 10^5$ Pa (atmospheric pressure) at the void, E_{inc} from (1) will be 4.32 kV/mm. The field magnitude at which the PD is quenched is known as the extinction electric field assumed $E_{ext} = 0.89$ kV/mm. The applied voltage is an 18 kV, 50 Hz sinusoidal voltage.

A. Simulation Results from the FEA Method

In the FEA model, COMSOL Multiphysics was integrated with MATLAB. The equations were coded in MATLAB while the electric field calculations were carried out in COMSOL.

Fig. 5 shows the algorithm developed in this paper for PD modeling based on the FEA method described in (1)-(21). At each time step, the FEA model is run to determine the state. When the state is 0, it means that the configuration is not undergoing PD, whereas the state at 1 declares that a PD is happening. At "state 0", when the two conditions for PD occurrence are satisfied, the algorithm switches to "state 1". At "state 1", once the electric field inside the cavity drops to E_{ext}, the PD quenches, and the system returns to "state 0". This procedure is continued until reaching the end of the period.

The parameters used for PD modeling through FEA are listed in Table I. The time steps between PD events, and during each of them are expressed as Δt_H and Δt_L, respectively. Preliminary results of the FEA developed was presented in [26, 27] and for silicone gel [28] by authors.

The model developed was run for 100 cycles and the results are reported in the second column of Table II under FEA.

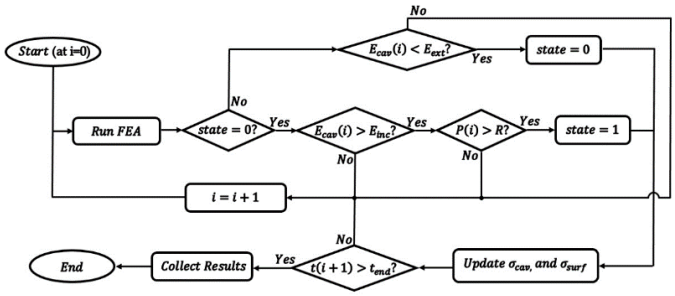

Fig. 5. Algorithm of PD modeling based on the FEA method developed.

TABLE I
Parameters used for PD modeling through the FEA method.

Symbol	Value [8, 13, 16, 17]	Symbol	Value [8, 13, 16, 17]
$(E/p)_{cr}$	24.2 $\mathrm{VPa^{-1}m^{-1}}$	$\sigma_{surf,H}$	2×10^{-11} S/m
B	8.6 $\mathrm{Pa^{1/2}m^{1/2}}$	Δt_H	$1/(1000\,f)$
n	0.5	Δt_L	1 ns
ϕ	1.3 eV	T	300 K
τ_{decay}	2 ms	γ	0.35
$\sigma_{void,0}$	0 S/m	ξ_+, ξ_-	1
$\sigma_{void,max}$	4×10^{-4} S/m	ν_0	10^{14} Hz
$\sigma_{surf,L}$	10^{-15} S/m		

TABLE II
Results derived by FEA and ICC methods

Variable / Method	FEA	ICC
Average number of PD per cycle	2.87	2.74
Mean true charge magnitude	745.09 pC	464.8 pC
Mean apparent charge magnitude	204.29 pC	169.62 pC
Maximum true charge magnitude	1985.6 pC	1330.8 pC

Fig. 6 shows the PRPD pattern for this case study. It should be noted that the code and model developed in this paper for the FEA method was first validated with experimental data in [11, 16-20].

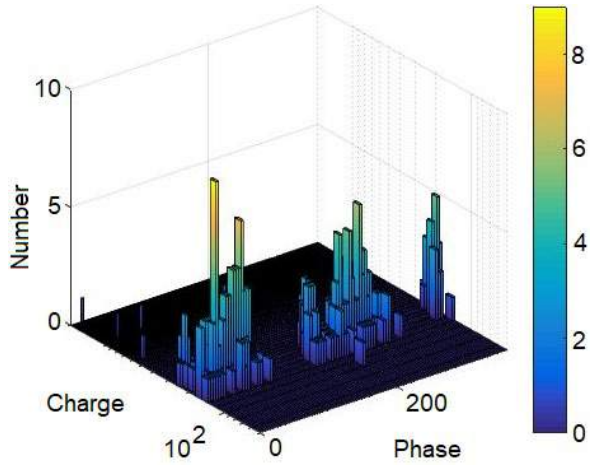

Fig. 6. The PRPD pattern resulted from the FEA model after 100 cycles.

B. Simulation Results from the ICC Method

The ICC model developed in this paper uses (22)-(31) with the parameters shown in Table I. Fig. 7 shows the electric field during two cycles of the applied voltage where f^*E_{out}, E_{inc}, and E_q are calculated by (34), (1), and (31), respectively. E_{cav} is calculated as the superposition of f^*E_{out} and E_q.

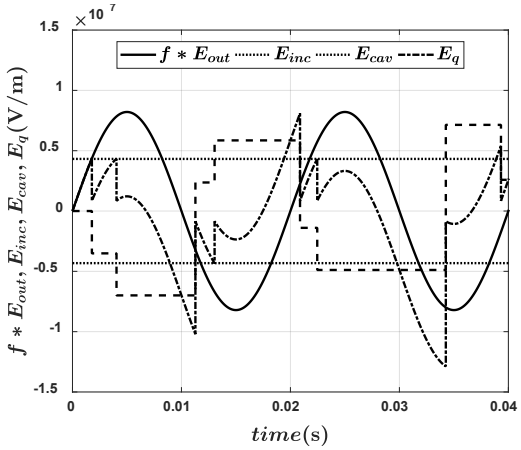

Fig. 7. f^*E_{out}, E_{inc}, E_q, and E_{cav} calculated by the ICC model developed.

Fig. 8a shows the real PD charge calculated by (28) during two cycles of the applied voltage. The minimum real PD charge (q_{min}) occurs at the first PD, where the void was discharged before starting the simulation. Fig. 8b shows the $q-\varphi-n$ diagram after 100 cycles of the applied voltage. As seen in Figs. 7, 8a, and 8b in the case of considerable time interval between two consecutive PD, when the polarity of E_{cav} between two consecutive PD events changes, the electron generation rate decreases due to the charge decay on the void surface and PD will occur when the magnitude of E_{cav} is much higher than E_{inc}, resulting in higher PD charge magnitudes. It should be noted that the code and model developed in this paper for the ICC method was first validated with experimental data in [11].

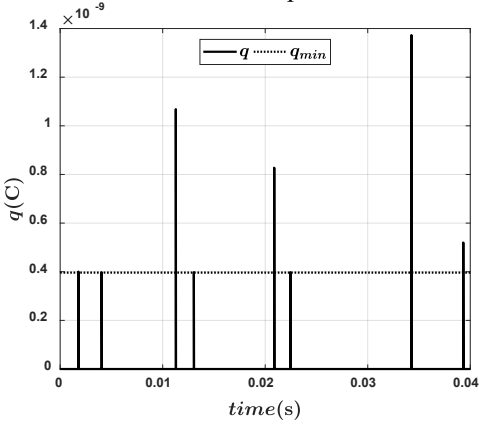

(a)

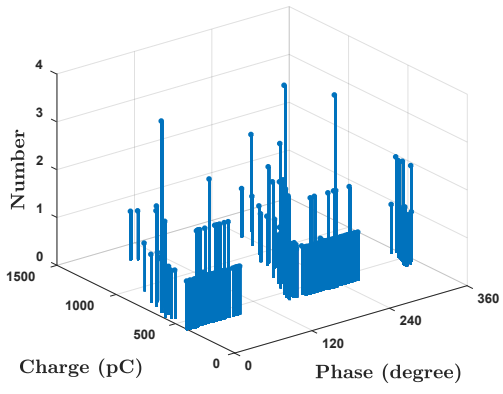

(b)

Fig. 8. a) Induced electric charge during the first two cycles of applied voltage. q_{min} is the minimum induced charge, b) Real electric charge $q-\varphi-n$ diagram after the first 100 cycles of the applied voltage.

The third column of Table II summarizes the minimum, mean and maximum values of the real and induced charge obtained in the simulation of the case study during 100 cycles of the applied voltage. As seen in Table II, the results obtained from these two methods are reasonably similar, however, the differences in maximum and mean magnitudes are due to different approaches used for modeling the surface charge decay process. The results obtained by the FEA model are more accurate since within the FEA model, fewer simplifications are performed to reach the ultimate result. For instance, there is no need in the FEA model to assume uniformity for the electric field either inside the void or in the dielectric; therefore, the results seem to be closer to reality.

It should be noted that, although detrapping of electrons from the surface of the solid insulator was considered in the model, other possible mechanisms and phenomena inside the bulk solid part near the void, due to space charges inside the void and surface charges on the void wall, has not been considered in the model. Indeed, the solid part was considered a perfect insulator. In addition, the effect on resultant electric field of free ends of the dipole chain in solid dielectric and molecular interactions should be considered. This is challenging technical gap and further research is needed to address it.

V. Sensitivity Analysis of Parameters

In this section, the variation of PD characteristics with respect to various parameters including void characteristics such as size and shape as well as environmental and electrical specifications such as air pressure and temperature inside the void, and void conductivity is assessed by the FEA model developed in this paper.

Fig. 9 shows the variation of apparent and true charges to changes in the void radius. The results simply imply that as the size of the void increases, the intensity of PD is escalated. This can be justified by mentioning that for larger voids, the void surface is larger. Moreover, the larger air gap needs higher electric field intensity to breakdown; therefore, it is expected that PD occurring at higher electric fields have higher intensities based on Ohm's law. Aside from the above reason, one should take into account the fact that the proximity of oppositely charged particles in the case of oblate voids makes the recombination of oppositely charged particles easier compared to the prolate voids. Thus, in the prolate voids, the chance of electron avalanche is much higher due to the availability of free electrons.

It is crystal clear that there are arbitrary shapes for voids which are hardly possible to be defined mathematically. However, in order to classify the voids and evaluate the impacts of each class on the occurrence of PD, different shapes for voids should be considered. In this regard, the original spherical shape examined in Section IV is generalized to a spheroidal shape, which can differ from an oblate to a prolate spheroid. An oblate void can be classified in the group of flat voids. On the other hand, the prolate shape can be assigned to the class of bar-shaped voids. It is assumed that during the changes in the void shape, its volume is kept constant.

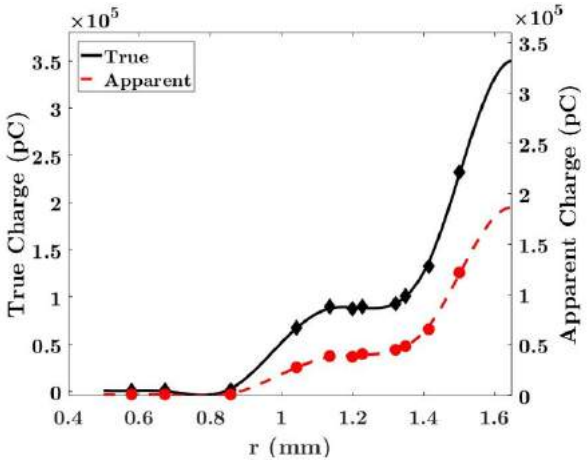

Fig. 9. Apparent and true charge magnitudes as functions of r.

Fig. 10 compares the apparent and true charge magnitudes of PD as a function of the vertical radius (r_z). The results indicate that the intensity of PD is enhanced in the case of prolate void rather than an oblate one. The latter conclusion can be reasoned through the longer air-gap along the electric field direction (z-direction). Hence, the long gap requires a higher electric field to break, and it is anticipated that at higher field intensities, the current density and, subsequently, the charge magnitudes have higher amounts.

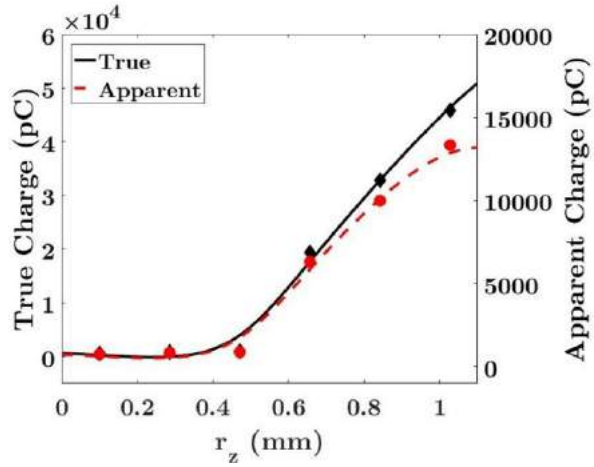

Fig. 10. Apparent and true charge magnitudes as functions of r_z.

Nowadays, electrification is penetrating various technologies such as aircraft, where one of the lesser-known parameters in the path toward electrification is pressure. During flights, an aircraft can undergo low-pressure conditions as low as 4 psi. Therefore, it is of great significance to delve into a reliability analysis of the insulation system under these severe conditions.

Different mechanisms within the PD-related processes depend on pressure. The inception electric field (E_{inc}) has an inverse relationship with pressure, meaning that as the pressure decreases, E_{inc} goes higher. However, one should not quickly infer that higher values lead to more resistance against PD threats; this is due to the higher magnitude of induced charge that the corresponding PD might have. Pressure also has an impact on the magnitude of the extinction electric field (E_{ext}). The latter conveys that at lower pressures, the electric field at which PD is quenched becomes lower than the expected value.

Fig. 11 shows the variations of E_{inc} and E_{ext} as functions of pressure. Subsequently, the duration of PD can be prolonged based on these changes. Furthermore, considering the ideal gas law and assuming a constant volume for voids over time, the temperature of the gas (air) can linearly change with the variation of pressure. Temperature can indirectly affect the PD characteristics by changing the exponential term in surface emission. To address the impact of pressure variation on PD characteristics, the PD analysis has been performed for different pressures.

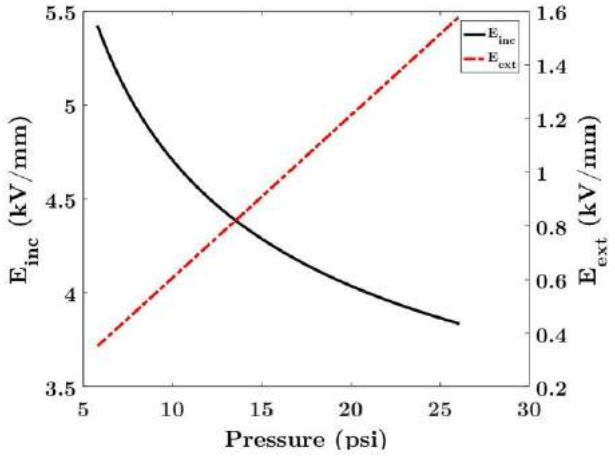

Fig. 11. Inception and extinction electric fields as functions of pressure.

Fig. 12 shows the variation of apparent PD charge magnitudes with pressure. The figure implies that below the atmospheric pressure, the electric field is somewhat saturated at a relatively high value. However, as the pressure exceeds the atmospheric pressure, the PD charges start to decline until about 20 psi, which is 50% above the atmospheric pressure. After that, the PD charges remain almost constant as the pressure increases.

There is no doubt that different parameters of the FEA model can affect the characteristics of PD, such as charge magnitudes, duration, and extinction time. One of these parameters is the conductivity of air during PD occurrence. Fig. 13 shows the PD charge magnitudes as a function of air conductivity where both PD charges increase when the void conductivity enhances during PD activities. This phenomenon can also be justified by Ohm's law despite the fact that a higher conductivity value leads to a more rapid electric field drop during PD.

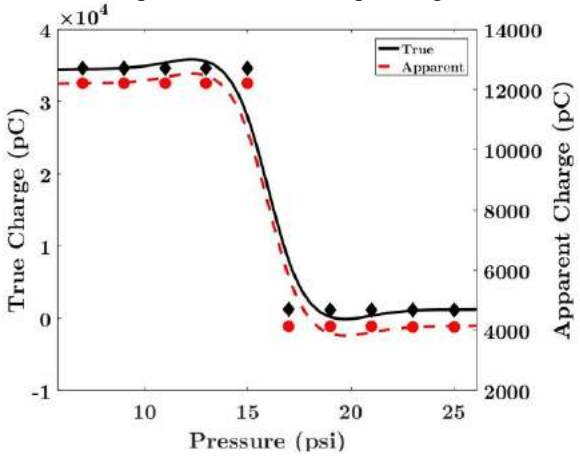

Fig. 12. Apparent and true charge magnitudes as functions of pressure.

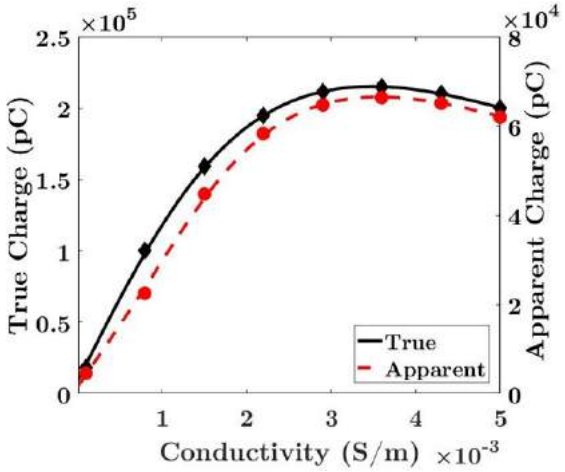

Fig. 13. Apparent and true charge magnitudes as functions of $\sigma_{void,max}$.

VI. Conclusions

In this paper, ICC and FEA methods for internal PD modeling were critically reviewed, delineated, developed, and coded in COMSOL Multiphysics integrated with MATLAB, where the originality of the proposed methods and analysis are:

- The ICC method was improved through introducing a new factor for calculating electrical field inside the void and;
- The sensitivity analysis of parameters carried out for the FEA method will help for evaluating the impact on PD phenomena when variables such as radius of the void, pressure and conductivity of the air will vary.

All equations employed in both methods were critically discussed. In FEA, a time-stepping method to indicate the state of PD at each time instant with the aid of inception and extinction conditions was developed. The simulation results in the same case study, obtained from both ICC and FEA methods, including $\boldsymbol{q-\varphi-n}$ diagram, were analyzed and compared. Moreover, the impact of various parameters on the PD characteristics was studied. For instance, it was observed that by reducing the radius of the void from 1.5 mm to 1.0 mm, the PD charge magnitude could be reduced by 50%. The influence of pressure on PD phenomena was also studied; although higher pressure can lead to a prolonged PD, the magnitude of PD apparent charge can be reduced by three times. It was also found that the conductivity of air during PD could cause an increase in the intensity of PD for more than five times.

VII. Acknowledgment

The material presented by Moein Borghei and Mona Ghassemi in this paper is based upon work supported in part by the Air Force Office of Scientific Research under award number FA9550-20-1-0033 and in part by the National Science Foundation under award number 1942540.

References

[1] M. Ghassemi, "Accelerated insulation aging due to fast, repetitive voltages: A review identifying challenges and future research needs," *IEEE Trans. Dielectr. Electr. Insul.*, vol. 26, no. 5, pp. 1558–1568, 2019.

[2] M. Mahdipour, A. Akbari, P. Werle, and H. Borsi, "Partial discharge localization on power cables using on-line transfer function," *IEEE Trans. Power Del.*, vol. 34, no. 4, pp. 1490–1498, 2019.

[3] K. Firuzi, M. Vakilian, B. T. Phung, and T. R. Blackburn, "Partial discharges pattern recognition of transformer defect model by LBP &

HOG features," *IEEE Trans. Power Del.*, vol. 34, no. 2, pp. 542–550, 2019.
[4] R. Albarracín, J. Ardila-Rey, and A. Masud, "On the use of monopole antennas for determining the effect of the enclosure of a power transformer tank in partial discharges electromagnetic propagation," *Sensors*, vol. 16, no. 2, 2018.
[5] H. Janani, B. Kordi, and M. Jafari Jozani, "Classification of simultaneous multiple partial discharge sources based on probabilistic interpretation using a two-step logistic regression algorithm," *IEEE Trans. Dielectr. Electr. Insul.*, vol. 24, no. 1, pp. 54–65, 2017.
[6] U. F. Khan, P. I. Lazaridis, H. Mohamed, R. Albarracín, Z. D. Zaharis, R. C. Atkinson, C. Tachtatzis, and I. A. Glover, "An efficient algorithm for partial discharge localization in high-voltage systems using received signal strength," *Sensors*, vol. 18, no. 11, 2016.
[7] S. Whitehead, *Dielectric Breakdown in Solids*, Oxford: Clarendon Press, 1951.
[8] G. C. Crichton, P. W. Karlsson, and A. Pedersen, "Partial discharges in ellipsoidal and spheroidal voids," *IEEE Trans. Dielectr. Electr. Insul.*, vol. 24, no. 2, pp. 335–342, 1989.
[9] G. Callender, T. Tanmaneeprasert, and P. L. Lewin, "Simulating partial discharge activity in a cylindrical void using a model of plasma dynamics," *J. Phys. D: Appl. Phys.*, vol. 52, no. 5, 2019.
[10] G. Callender, I. O. Golosnoy, P. Rapisarda, and P. L. Lewin, "Critical analysis of partial discharge dynamics in air filled spherical voids," *J. Phys. D: Appl. Phys.*, vol. 51, no.12, 2018.
[11] H. A. Illias, G. Chen and P. L. Lewin, "Comparison between three-capacitance, analytical-based and finite element analysis partial discharge models in condition monitoring," *IEEE Trans. Dielectr. Electr. Insul.*, vol. 24, no. 1, pp. 99–109, 2017.
[12] C. Pan, G. Chen, J. Tang, and K. Wu, "Numerical modeling of partial discharges in a solid dielectric-bounded cavity: A review," *IEEE Trans. Dielectr. Electr. Insul.*, vol. 26, no. 3, pp. 981–1000, 2019.
[13] L. Niemeyer, "A generalized approach to partial discharge modeling," *IEEE Trans. Dielectr. Electr. Insul.*, vol. 2, no. 4, pp. 510–528, 1995.
[14] R. Schifani, R. Candela and P. Romano, "On PD mechanisms at high temperature in voids included in an epoxy resin," *IEEE Trans. Dielectr. Electr. Insul.*, vol. 8, no. 4, pp. 589–597, 2001.
[15] F. Gutfleisch and L. Niemeyer, "Measurement and simulation of PD in epoxy voids," *IEEE Trans. Dielectr. Electr. Insul.*, vol. 2, no. 5, pp. 729–743, 1995.
[16] H. Illias, G. Chen, and P. L. Lewin, "Partial discharge behavior within a spherical cavity in a solid dielectric material as a function of frequency and amplitude of the applied voltage," *IEEE Trans. Dielectr. Electr. Insul.*, vol. 18, no. 2, pp. 432–443, 2011.
[17] C. Forssen and H. Edin, "Partial discharges in a cavity at variable applied frequency part 2: measurements and modeling," *IEEE Trans. Dielectr. Electr. Insul.*, vol. 15, no. 6, pp. 1610–1616, 2008.
[18] H. A. Illias, G. Chen, and P. L. Lewin, "The influence of spherical cavity surface charge distribution on the sequence of partial discharge events," *J. Phys. D: Appl. Phys.*, vol. 44, no. 24, 245202, Jun. 2011.
[19] H. A. Illias, G. Chen, A. H. A. Bakar, H. Mokhlis, and M. A. Tunio, "Partial discharges within two spherical voids in an epoxy resin," *J. Phys. D: Appl. Phys.*, vol. 46, p. 335301, 2013.
[20] H. A. Illias, G. Chen, and P. L. Lewin, "Partial discharge within a spherical cavity in a dielectric material as a function of cavity size and material temperature," *IET Sci., Meas. & Technol.*, vol. 6, no. 2, pp. 52–62, 2012.
[21] A. Pedersen, "Partial discharges in voids in solid dielectrics: An alternative approach," in *Proc. Annu. Rep. Conf. Electr. Insul. Dielectr. Phenom. (CEIDP)*, 1987, pp. 58–64.
[22] S. A. Boggs, "Partial discharge. III. Cavity-induced PD in solid dielectrics," IEEE Electr. Insul. Mag., vol. 6, no. 6, pp. 11–16, 1990.
[23] E. Lemke, "A critical review of partial-discharge models," *IEEE Electr. Insul. Mag.*, vol. 28, no. 6, pp. 11–16, 2012.
[24] T. Tanaka, "Internal partial discharge and material degradation," *IEEE Trans. Electr. Insul.*, vol. EI-21, no. 6, pp. 899–905, 1986.
[25] E. Lemke, "Analysis of the partial discharge charge transfer in extruded power cables," *IEEE Electr. Insul. Mag.*, vol. 29, no. 1, pp. 24–28, 2013.
[26] M. Borghei and M. Ghassemi, "Finite element modeling of partial discharge activity within a spherical cavity in a solid dielectric material under fast, repetitive voltage pulses," in *Proc. IEEE Electr. Insul. Conf. (EIC)*, 2019, pp. 34–37.
[27] M. Borghei and M. Ghassemi, "Partial discharge finite element analysis under fast, repetitive voltage pulses," in *Proc.* IEEE Electr. Ship Technol. Symp. (ESTS), 2019, pp. 324–328.
[28] M. Borghei and M. Ghassemi, "Partial discharge analysis under high-frequency, fast-rise square wave voltages in silicone gel: A modeling approach," *Energies*, vol. 12, no. 23, 2019.

Moein Borghei (S'18) received his B.Sc. degree in electrical engineering, power system/electronics (Hons.) from Sharif University of Technology, Tehran, Iran in 2018. He is currently working toward his Ph.D. in the ECE Dept. at Virginia Tech. His research interests include power system resiliency, power system analysis, transmission line design, and dielectrics and electrical insulation.

Mona Ghassemi (S'07–M'13–SM'16) received her M.Sc. and Ph.D. degrees (Hons.) in electrical engineering from the University of Tehran, Tehran, Iran, in 2007 and 2012, respectively. She spent two years (2013-2015) researching as a Post-Doctoral Fellow at the High Voltage Laboratory of the University of Quebec, QC, Canada. She was also a Post-Doctoral Fellow at the Electrical Insulation Research Center, Institute of Materials Science, University of Connecticut, Storrs, CT, USA, from 2015 to 2017. In 2017, she joined the ECE Department at Virginia Tech (Blacksburg, VA, USA) as an Assistant Professor. Dr. Ghassemi is an At-Large Member of the Administrative Committee of the IEEE Dielectrics and Electrical Insulation Society for 2020–2023, a Corresponding Member of the IEEE Conference Publication Committee of the IEEE Power & Energy Society, an Active Member of several CIGRE working groups and IEEE Task Forces, and a member of the Education Committee of the IEEE DEIS and PES. She is a registered Professional Engineer in the Province of Ontario, Canada, and an Associate Editor of the *IEEE Transactions on Industry Applications,* the *IET High Voltage,* and the *International Journal of Electrical Engineering Education*. She is also a recipient of the 2020 National Science Foundation (NSF) CAREER Award and the 2020 Air Force Office of Scientific Research (AFOSR) Young Investigator Research Program (YIP) Award. Her research interests include electrical insulation materials and systems, high voltage/field technology, Multiphysics modeling, electromagnetic transients in power systems, and power system analysis and modeling.

Johnatan M. Rodríguez-Serna received the B.Eng and M.Sc. degrees in 2007 and 2011, respectively, in electrical engineering from the Universidad de Antioquia. He is an Assistant Professor at the Electrical Engineering Department at the Universidad de Antioquia (UdeA). Currently, he is a PhD student since October 2018 at the Universidad Politécnica de Madrid (UPM). His main research interests include partial discharge modeling and measurement, high-voltage engineering, and electromagnetic compatibility.

Ricardo Albarracín-Sánchez received his B.Sc, M.Sc., and Ph.D. degrees in electrical engineering in 2008, 2010, and 2014, respectively, from the Universidad Carlos III de Madrid (UC3M), Spain. Currently, he is Associate Professor in electrical engineering field at Universidad Politécnica de Madrid (UPM). He is Vice-dean of Economic Affairs and Planning at School of Industrial Design and Engineering (ETSIDI)-UPM where he was Assistant to the Director for International Mobility (Erasmus+ School coordinator). He works as international researcher in Electrical Engineering topics at ETSIDI-UPM collaborating with international universities all around the world. He worked for Gas Natural Fenosa (Naturgy) being leader in Innovation, Technology and R&D in the electrical grids and generation area at Boslan Ingeniería Consultoría. Besides, he worked as Adjunct Professor at Universidad Pontificia de Comillas. He also worked at Universidad Politécnica de Madrid as postdoc and at Universidad Carlos III de Madrid as Assistant Professor. His main research interest areas are electrical insulation, insulating polymers, modeling weaknesses in insulation systems, partial discharges, condition monitoring, UHF sensors, nanodielectrics, power transformers, and renewable energy.

Anexo C: publicación complementaria O3-1C

En este anexo se presenta la publicación complementaria O3-1C, ver Figura 12 y Sección 5.2.4.4 en Capítulo 5. En el siguiente cuadro se resumen el título del trabajo, los autores, el nombre del evento, el lugar, y su ISBN. Además, se agrega información general del artículo de congreso, como el año y rango de páginas, si es o no de acceso abierto, el DOI, las palabras clave y el resumen en inglés.

Publicación	O3-1C	
Título	Simulation of Polymeric Insulators Ageing Induced by the Impact Energy of Electrons During Partial Discharge Activity	
Autores	Johnatan M. Rodríguez-Serna y Ricardo Albarracín-Sánchez	
Universidades colaboradoras	Universidad Politécnica de Madrid	
Evento	2021 IEEE Texas Power and Energy Conference (TPEC)	
Lugar	College Station, TX, USA	
ISBN	978-1-7281-8612-2	
Año, páginas	2021, 6	
DOI	**10.1109/TPEC51183.2021.9384986**	
Publicación de acceso abierto	Sí	
	No	X
Keywords	Aging, partial discharges, polymers, prognosis	
Abstract	The economic and reliable sizing of High-Voltage (HV) insulation systems requires the evaluation of the expected life when they are under normal stresses. However, when solid dielectric polymers are used, organic materials in general, Partial Discharges (PDs) activity in cavities inside the dielectric bulk accelerates the aging process due to chemical and physical degradation mechanisms. On the other hand, prognosis tools based on external PD measurements are required in order to take decisions about the maintenance actions. In this work, a study on the degradation rate driven by the impact energy of electrons during PDs, a method based on simulations and a proposed degradation function are presented. Comparisons of calculated life obtained from measurements show good agreement. Additionally, a diagnostic quantity based on the induced PD current is proposed.	

Simulation of Polymeric Insulators Ageing Induced by the Impact Energy of Electrons During Partial Discharge Activity

Johnatan M. Rodríguez-Serna
Dept. of Electrical and Electronic Engineering, Automatic Control and Applied Physics
Universidad Politécnica de Madrid, ETSIDI
Madrid, Spain
johnatan.rodriguez.serna@alumnos.upm.es

Ricardo Albarracín-Sánchez
Dept. of Electrical and Electronic Engineering, Automatic Control and Applied Physics
Universidad Politécnica de Madrid, ETSIDI
Madrid, Spain
ricardo.albarracin@upm.es

2021 IEEE Texas Power and Energy Conference (TPEC) | 978-1-7281-8612-2/21/$31.00 ©2021 IEEE | DOI: 10.1109/TPEC51183.2021.9384986

***Abstract*—The economic and reliable sizing of High-Voltage (HV) insulation systems requires the evaluation of the expected life when they are under normal stresses. However, when solid dielectric polymers are used, organic materials in general, Partial Discharges (PDs) activity in cavities inside the dielectric bulk accelerates the ageing process due to chemical and physical degradation mechanisms. On the other hand, prognosis tools based on external PD measurements are required in order to take decisions about the maintenance actions. In this work, a study on the degradation rate driven by the impact energy of electrons during PDs, a method based on simulations and a proposed degradation function are presented. Comparisons of calculated life obtained from measurements show good agreement. Additionally, a diagnostic quantity based on the induced PD current is proposed.**

Keywords—ageing, partial discharges, polymers, prognosis

I. Introduction

Solid polymeric materials are used as insulation systems in many applications from electronics to power equipment in High Voltage (HV) [1]. Epoxy resins exhibit optimal characteristics for insulation systems manufacturing in power equipment, such as good adhesion, minimal shrinkage during curing and none volatile by-products produced during the curing [2]. Due to insulation systems manufacturing processes, cross-linking and curing dynamics, micro cavities can appear in the dielectric bulk [3] where PDs can be incepted. PDs produce local degradation that leads to a final dielectric breakdown through the formation of pits and craters on the cavity surface where a tree can be incepted because of local field enhancement [2]. PDs erode and degrade the dielectric material through the following physical and chemical mechanisms [3]–[5]:

- Bombardment of the surface by highly energetic charge carriers and photons;
- Local temperature rising by high-temperature discharge gases; and
- Chemical reactions started by excited molecules and/or chemical compound in the gas (particularly oxygen and ozone) and solid phase.

The continuous ion bombardment of the surface in oxygen free conditions is able to produce craters or pits, but under normal conditions it only appears as a worsening factor of existing damage [3]. Similarly, the local temperature rising can accelerates the chemical reactions, but other thermal degradation mechanisms, such as the direct melting, are negligible [6].

On the other hand, highly-energetic charge carriers accelerated by the local electric field, hot electrons, and ultraviolet (UV) radiation produced during PDs collide with gas and polymer molecules causing chain scission in the polymeric matrix through Dissociation by Electron Attachment (DEA) [7]. This chemical mechanism is the most obvious for polymer degradation driven by PDs in cavities [8].

As the latter is the fastest degradation mechanism, specially, in organic materials or oil-paper [9], PDs measured parameters can be used as effective diagnostic quantities in microscopic life models for developing prognosis tools [10], which allows to improve the reliability of electrical assets and the effectiveness of maintenance actions.

In this paper, the impact energy of electrons produced during PDs in air filled spherical cavities within epoxy resin, calculated using a partial discharge (PD) model based on the Finite-Element Method (FEA) and analytical expressions at different ageing phases, is shown. The induced degradation by DEA into the polymer and the time-to-breakdown (life) are evaluated using a proposed damage function and the PD simulation results obtained. In addition, PDs measured parameters are evaluated as diagnostic quantities related to the degradation induced by the impact energy during PDs.

The paper is organized as follows: first, the simulation models and methods are presented in section II, then the case of study and simulation results are presented and discussed in section III. Finally, some conclusions are drawn in section IV.

II. Models and Method for Life Calculation

Taking into account theoretical and experimental studies [11], [12], it is assumed that PDs activity in spherical cavities

978-1-7281-8612-2/21/$31.00 ©2021 IEEE

can incept treeing, being the last stage of the ageing process before breakdown.

The PD activity behavior along the ageing period changes, which means that the ageing rate and the degradation mechanism can be different. However, here it is assumed that the chemical mechanism driven by PDs is the predominant along the ageing period considered [13].

Besides, it is assumed that the insulation life, once PDs activity into cavities have been initiated, corresponds to the time required until a channel is generated from the surface of the cavity in which the PDs can be self-sustained, i.e. independent of the discharges in the cavity, and the propagation of the electrical trees is incepted [14]. The life is considered to be approximately equal to the time required for tree inception, which in practice is approximately equal to the time-to-breakdown [15].

The method for calculating the ageing induced by PDs in spherical cavities within solid dielectrics is composed by two steps:

- PDs simulation; and
- PD induced damage calculation.

In the first step, PDs are simulated using the hybrid PD-FEA model presented in [16]. During PDs activity, the impact energy acquired by the electrons is calculated as a function of the electric field strength magnitude inside the cavity and the cavity gas temperature and pressure. Taking into account that the mean free path, and also the electrons mobility, in air and nitrogen are quite similar [17], it is assumed that the cavity gas is air along the ageing period considered [18].

In the second step, the damage done to the solid dielectric by PDs activity is calculated as a function of the PD-electrons energy distribution and the scattering rates in the polymer [19].

A. PD Induced Degradation and Life Calculation

The degradation of polymeric materials is the result of an energy transformation process. A fraction of the energy supplied to electrons in the PD avalanches is required to vaporize the polymer through DEA [20]. DEA is a process where electrons are temporarily trapped in a resonant state of the molecules (*AB*) and if the energy of electrons is higher than a threshold value (~8 eV for polymers) and the resonance is long-enough, molecules are fragmented [21]. This process can be schematically represented as:

$$AB + e^- \rightarrow A + B^- \; or \; A^- + B \tag{1}$$

In low-energy plasmas, DEA is the initial step for radicals and ions generation. Here it is assumed that DEA is activated by the impact energy of charge carriers [22].

Assuming a Maxwell distribution of the electrons drift velocity and single avalanches along the cavity diameter, the impact energy of the electrons colliding with the polymeric surface during the *i*-th PD is given by [22]:

$$W_{el}^i = 13.1 m_{el} N_{el}^i \left(v_{el}^i (E_{cav}^i, p) \right)^2, \tag{2}$$

where m_{el} (kg) is the electron rest mass (9.1×10^{-31} kg), $N_{el}^i = q_{PD}^i / q_0$, is the number of electrons in the *i*-th PD, q_{PD}^i (C) is the charge magnitude of the *i*-th PD, q_0 (C) is the elementary charge (1.6×10^{-19} C), E_{cav}^i (V·m^{-1}) is the electric field strength magnitude inside the cavity during the *i*-th PD, p (Pa) is the cavity gas pressure and v_{el}^i (m·s^{-1}) is the electrons drift velocity calculated for standard atmospheric conditions as follows [23]:

$$v_{el}^i = 60.6 (E_{cav}^i / 100)^{0.75} \tag{3}$$

Taking into account that the electric field strength magnitude inside the cavity and the electron drift velocity are reduced during the PD, the average impact energy during the *i*-th PD is calculated as follows:

$$\underline{W_{el}^i} = \frac{1}{E_{cav}(t_{PD}^i) - E_{Ext}} \int_{E_{Ext}}^{E_{cav}(t_{PD}^i)} W_{el}(E_{cav}) dE_{cav} \tag{4}$$

where $E_{cav}(t_{PD}^i)$ (V·m^{-1}) is the electric field strength magnitude in the cavity at the inception of the *i*-th PD and E_{Ext} (V·m^{-1}) is the extinction field strength magnitude.

The energy density acquired by the gas molecules by collisions with electrons, reaches its maximum in front of the cathode center. For this reason, dissociation by-products in the gas will be concentrated at the cathode [24]. On the other hand, electrons dissipate their kinetic energy at the anode on the cavity surface and the gas molecules close to it. Chemical reactions in the gas phase will be concentrated in the cathode, but their participation against chemical reactions in the solid, is almost negligible [25].

The relevant fraction of energy for activating chemical processes at energies higher than W_{lim} (eV), the minimum magnitude of energy enough for starting chemical reactions, can be calculated as follows [26]:

$$f(W > W_{lim}) = \frac{2}{\sqrt{\pi}} (W_{lim}/kT)^{0.5} \exp(-W_{lim}/kT) \tag{5}$$

where k (eV·K^{-1}) is the Boltzmann constant and T (K) the temperature. For DEA in polymers W_{lim}=8 eV. The effective energy for producing polymer degradation can be calculated as the product of (4) by (5). The impact energy density on the cavity surface can be calculated as follows:

$$\underline{w_{el}^i} = 0.2 \left(\underline{W_{el}^i} / S_{cav} \right) f \left(\underline{W_{el}^i} > W_{lim} \right) \tag{6}$$

where S_{cav} (m^2) is the area of the cavity surface where the electrons in PDs collide. From observations in [27], S_{cav} is assumed as $2\pi a^2 \int_0^{\pi/4} sen\theta d\theta$. a (m) is the cavity radius and 0.2 is the fraction of hot-electrons effective in dissociating the C-H bonds [19]. The vaporization energy for dissociating the C-H bonds in a cylinder with radius R=10 μm and the lamella length D_{dis}= 400 Å at the cavity-gas interface can be calculated as follows:

$$W_V = w_V \pi R^2 D_{dis} \tag{7}$$

where w_V=7.56x10^{10} (J·m^{-3}) is the vaporization energy density [28]. A damage function dependent on the impact energy can be defined as follows:

$$f_{PD}^{i} = \left(\underline{w_{el}^{i}}/W_V\right)\pi R^2 \quad (8)$$

Due to the continuous PD activity, the damage accumulates until the C-H bonds in the cylinder of radius R and length D_{dis} are dissociated, then $\sum f_{PD}^{i}$=1 and the time will be equal to t_{dis} s. Considering that d_c=10 μm is the critical length from which an electrical tree can be started and propagates independently from the PDs activity at the cavity [29], the life, L (s), is calculated as follows:

$$L = d_c t_{sim}/D_{dis}\sum_{t_{sim}} f_{PD}^{i} \quad (9)$$

where $\sum_{t_{sim}} f_{PD}^{i}$ is the accumulated damage during the simulation time t_{sim} (s).

The impact energy produce local heating, chain scission, formation of radicals and cross-linking [24], but unfortunately cannot be directly determined using PDs measured parameters, mainly because it depends on the electric field strength inside the cavity. An approximate estimation can be done using the following approach. Modelling the PDs as consecutive electron avalanches in the cavity gas along the cavity diameter, d (m), the charge, q (C), after an avalanche corresponds to:

$$q = q_0 N_0 \exp[(\alpha - \eta)d] \quad (10)$$

where N_0 is the initial number of electrons at the avalanche inception and α (m^{-1}) and η (m^{-1}) are, respectively, the first and second Townsend coefficients [17]. The dipole moment in C·m can be expressed as follows [30]:

$$\mu = [q_0 N_0/(\alpha - \eta)]\exp[(\alpha - \eta)d] \quad (11)$$

The induced PD charge can be calculated as $q' = \mu\nabla\lambda$ (C), where $\nabla\lambda$ (m^{-1}) is the electric field strength magnitude at the center of the cavity per unit of applied voltage [31]. The induced PD current, calculated as the time derivative of the induced charge, is:

$$i' = q_0 N_0 v_{el}\nabla\lambda\exp[(\alpha - \eta)v_{el}] \text{ for } 0 \le t \le d/v_{el} \quad (12)$$

As the first electron avalanche gives the peak current and the drift velocity in the resultant electric field is drastically reduced by the field generated by the surface charge density, the average electron drift velocity can be approximated to:

$$\underline{v_{el}} \cong i'_{max}/(q_{PD}\nabla\lambda) \quad (13)$$

Taken into account (2) and (13), the impact energy can be rewritten as follows:

$$W_{el}^{i} \cong 13.1 m_{el} v_{el}\left(E_{cav}\left(t_{PD}^{i}\right), p\right) i'_{max}/(q_0\nabla\lambda) \quad (14)$$

Equation (14) allows concluding that the impact energy of electrons is proportional to the peak value of the PD current. However, it must be taken into account that the drift velocity is dependent on the cavity gas pressure and the electric field strength magnitude in the cavity. In (14), it was assumed that the largest electron avalanche propagates with a velocity determined by the electric field strength magnitude at the PD inception. Besides, measurements in spherical voids filled with air at atmospheric conditions in epoxy resins allowed to conclude that there is a correlation between the measured peak current and the PD impact energy [22].

III. Simulation Results and Discussion

The case of study is the same as that considered in [16] and [18], and it is shown in the Fig. 1. It corresponds to an air-filled spherical cavity, of 2.5 mm diameter ($2a$) in the center of a linear, homogenous, and isotropic dielectric bulk of epoxy resin (Araldit D/HY 956) of 3.5 mm thickness between two parallel plates. A 19.25 kV, 50 Hz sinusoidal voltage source is applied to the upper electrode while the lower one is grounded. The ratio of the applied voltage to the streamer inception voltage was 3.7. PD measurements were taken using a commercial PD analyzer (Power Diagnostix ICM) implementing the IEC 60270 PD measuring circuit with a sensitivity of 0.5 pC. Simulations were implemented for five consecutive periods (phases) during different ageing stages: Phase A, from unaged to 0.17 h; Phase B, from end of Phase A to 35.17 h; Phase C, from end of Phase B to 185.17 h; Phase D, from end of Phase C to 1235 h and Phase E, from end of Phase D to 1285 h.

The ageing phases were defined that way according to the changes of the PD behavior during the time under stress, age [18]. The parameters of media and the PD simulation model for each ageing phase are presented in [16] and [18]. Thirty simulations were carried out for each ageing phase during 500 cycles of the AC applied voltage. Typical simulation results for the Phase-Resolved PD (PRPD) pattern and the accumulated damaged are presented in Fig. 2.

In Fig. 2, $|q_{real}|$ (pC) corresponds to the magnitude of the real PD charge in the cavity and "Damage (A.U.)", is the value of the damage function accumulated during the simulation time calculated with (8). Table I, summarizes the maximum values during each ageing phase taken from the typical simulation results. The damage induced by the collision of electrons is accumulated at the center of the anode on the cavity surface, which under AC fields, alternates among the surfaces S_1, blue, and S_2, red in Fig. 1 and Fig. 2. depending on the polarity of the resultant electric field inside the cavity.

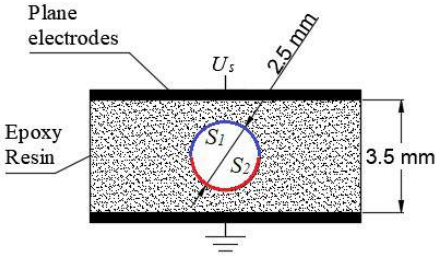

Fig. 1. Geometry of the case study, epoxy resin (Araldit D/HY 956) of 3.5 mm thickness between two parallel plates, voltage stress is 19.25 kV, 50 Hz.

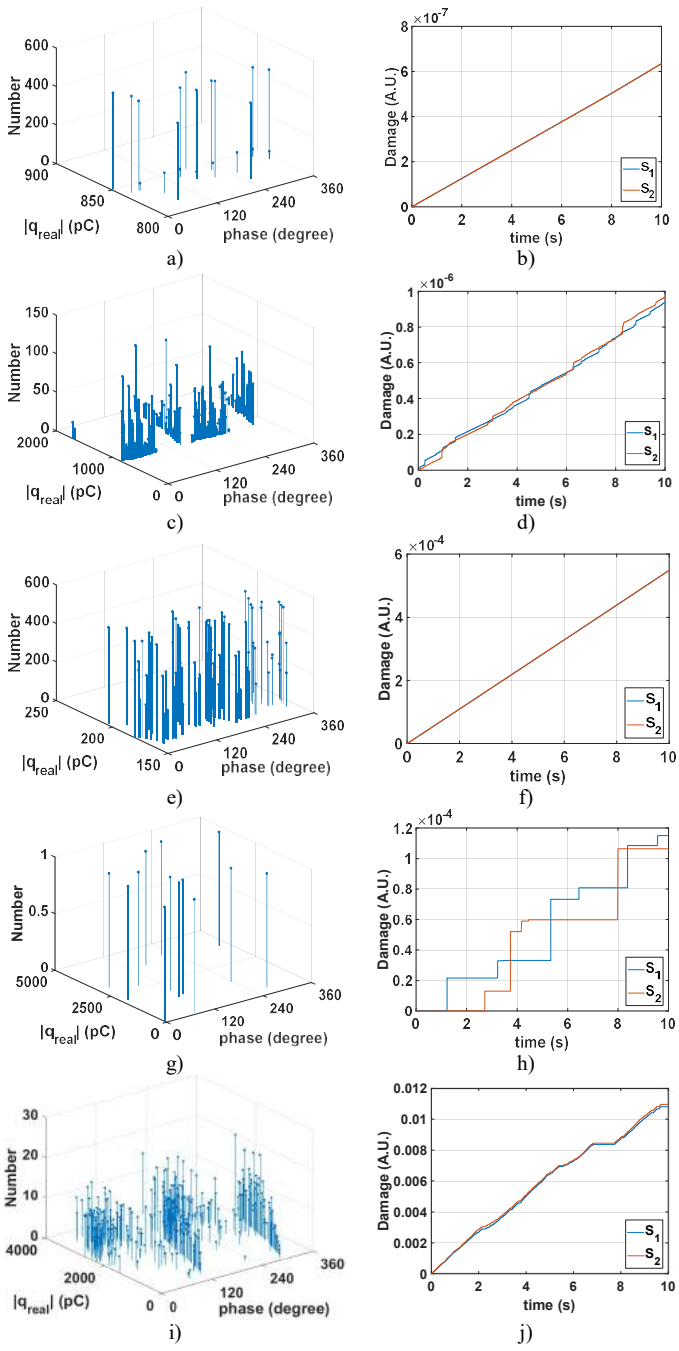

Fig. 2. Simulation results of PRPD pattern and accumulated damage function for the five ageing phases: a) and b), Phase A; c) and d), Phase B; e) and f), Phase C; g) and h), Phase D and i) and j), Phase E.

In Table I, $N_{HW\text{-}sim}$ and $N_{HW\text{-}meas}$ are, respectively, the number of PDs per half cycle, simulated and measured in [18] and *Diff* is the relative difference among these values. The maximum error was 24.4 % for Phase E. The validation of the simulation results and analysis of the error were presented in [16]. The induced current is calculated as the time derivative of the PD induced charge. In Table I, it can be seen that with ageing, except during phases C and D, the maximum values of PD charge and induced PD current increase. This same behavior can

TABLE I. SUMMARY OF THE SIMULATION RESULTS TAKEN FROM THE TYPICAL SIMULATION RESULTS

Ageing Phase	A	B	C	D	E
q_{max} (pC)	850.9	1944.8	205.2	4154.8	3859.2
q'_{max} (pC)	540.3	1234.8	130.3	2638.0	2450.3
i'_{max} (μA)	10.8	24.7	2.6	52.8	49.0
$\underline{W_{el}}_{max}$ (J)	$1.7\text{x}10^{-9}$	$1.0\text{x}10^{-8}$	$4.3\text{x}10^{-9}$	$6.1\text{x}10^{-5}$	$5.1\text{x}10^{-5}$
$N_{HW\text{-}sim}$	6	5.5	32.0	0.03	2.6
$N_{HW\text{-}meas}$	5 -7	~5.8	~30	0.03	~3
Diff (%)	14.3	5.3	6.7	0	24.4
$\alpha_{q'}$ (pC)	532.9	563.4	115.5	2200.1	988.1
$\alpha_{i'}$ (μA)	10.7	11.3	2.3	44.0	19.8
$\beta_{q'\text{-}i'}$	85.0	6.2	17.1	1.5	1.7

be seen for the maximum value of the impact energy, $\underline{W_{el}}_{max}$ (J). When comparing the simulation results for phases A and C, it can be seen that despite of the PD charge is higher for phase A than for phase C, the impact energy is higher for phase C than for phase A. This can be explained by the fact that with the ageing in the cavity, gas pressure diminishes causing the mean free path to increase and electrons can acquire higher kinetic energies even so under electric fields of lower magnitude. The latter allows concluding that the magnitude of the PD charge cannot be taken as a separate diagnostic quantity for evaluating the ageing conditions.

Additionally, the typical results for the induced PD charge and current at each ageing phase, q' (pC) and i' (μA), were fitted to the Weibull function using the maximum likelihood method [32], and the scale, $\alpha_{q'}$ (pC), $\alpha_{i'}$ (μA), and shape, $\beta_{q'-i'}$, parameters obtained are also shown in Table I. From the simulation results, and as it was suggested in [33], it can be seen that the value of the shape parameter tends to decrease with ageing and can be used as a good ageing indicator.

Life was calculated with (9) for each of the thirty simulations at the five ageing phases and the resultant distributions were also fitted to the Weibull function. The results are summarized in Table II, where the values between parentheses correspond to the 95 % confidence intervals. In the accumulated damage functions plotted in Fig. 2, it can be seen that the ageing rate driven by PDs is variable along the ageing phases and the Miner law [34] can be used for calculating the time-to-breakdown, life, under the last of the five ageing phases as follows:

$$\sum_j t_{age}^j / L_j = 1 \qquad (15)$$

TABLE II. PARAMATERS OF THE WEIBULL FUNCTION FITTED TO THE LIFE SIMULATION RESULTS

Ageing Phase	A	B	C	D	E
t_{age} (h)	0.2	35.0	150.0	1049.8	50
α_L (h)	$1.1\text{x}10^6$ ($1.1\text{x}10^6$-$1.1\text{x}10^6$)	$7.9\text{x}10^5$ ($7.8\text{x}10^5$-$8.1\text{x}10^5$)	$1.3\text{x}10^3$ ($1.3\text{x}10^3$-$1.3\text{x}10^3$)	$4.8\text{x}10^3$ ($3.5\text{x}10^3$-$6.6\text{x}10^3$)	78.4 (75.2-81.7)
β_L	Inf (Inf-Inf)	19.4 (14.9-25.3)	Inf (Inf-Inf)	1.2 (0.9-1.5)	9.3 (7.1-12.1)

where t_{age}^{i} (h) is the part of the life time corresponding to the duration of the j-th ageing phase and L_j (h) is the life calculated during the j-th ageing phase. Using (15) and the results in Table II, the life corresponds to L_5=51.9 (43.7 – 59.0) h. The values between parentheses were calculated using the confidence intervals in Table II. As the duration of the last phase is 50 h, the breakdown would occur between 1.9 h to 9 h after the end of the final ageing phase or 6.3 h before the end of the final ageing phase. Authors in [18], reported that tree inception was detected ~15 h after the end of the last ageing phase (~1300 h from unaged), i.e. the simulation results exhibit a difference of about 6 to 13 h (1287 h to 1294 h from unaged) with respect to the measured ones. This allows inferring that the proposed damage function and method are reliable and permit to evaluate quantitatively the ageing conditions induced by PDs. It must be noted here that despite of the good results, the values obtained using the method presented in this paper should be regarded as mere quantitative inferences because the effect of other degradation mechanisms at different ageing phases must be also considered. For instance, at the initial ageing stages, in oxygen rich conditions, a synergy exists between DEA and autoxidation [35]. On the other hand, in oxygen free conditions, the lamella at the gas-solid interface is subjected to the direct attack of hot electrons and UV radiation, which gradually decomposes it and a small channel is formed initiating a tree. Furthermore, the by-product deposition and charge carrier bombardment modify the cavity surface conductivity and roughness as well as the cavity morphology, crystals are formed on the cavity surface [36], which affect the PD behavior and indeed the degradation rate.

It is clear that the precise damage evaluation requires the precise quantification of the PD energy. However, it cannot be calculated using the external PD measured parameters [22]. From (13) and (14) it is clear to conclude that the peak value of the induced PD current can be related to the impact energy of electrons during PDs activity. In [37], it was concluded that the product $N_{PD}\alpha_{q'}$, where $N_{PD} = 2N_{HW}$ is the number of PDs per cycle, gives a measure of the average rate of electrons colliding with the polymeric surface per cycle and is related to the amount of energy dissipated by the discharges during each voltage cycle. The value $\underline{N_{PD}\alpha_{q'}}$, calculated as the average accumulated during the ageing phases, indicates the average ageing rate.

On the other hand, taking into account the relationship between electrons drift velocity and PD current, see (13), here it is proposed the value $\underline{N_{PD}(\alpha_{i'})^2}$ as indicative of the ageing rate. The relationship between time and life in (15) is by definition proportional to the accumulated damage ($\underline{AD}$). Fig. 3, shows a comparison between the magnitudes of $\underline{AD}$=$\sum_1^j t_{age}^j / L_j$, $\underline{N_{PD}\alpha_{q'}}$ and $\underline{N_{PD}(\alpha_{i'})^2}$ calculated using the values presented in Table I and Table II, normalized to their relative maximum values.

In Fig. 3, it can be seen that the dielectric is highly degraded during the two last ageing phases, where the PD charge and current are the maximal. On the other hand, it can be seen that the value of the $\underline{N_{PD}(\alpha_{i'})^2}$ increases continuously in the same proportion as the accumulated damage, $\underline{AD}$, decreases and therefore, the life increases. For this reason, the value of $\underline{N_{PD}(\alpha_{i'})^2}$ along ageing is indicative of the average ageing rate

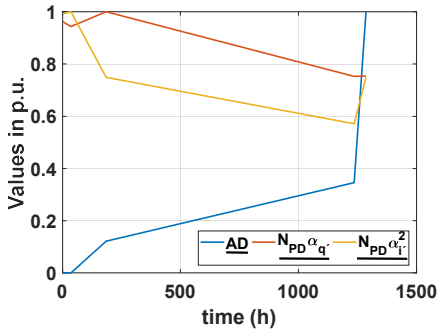

Fig. 3. Comparison of accumulated damage and ageing rate functions.

and, compared with $\underline{N_{PD}\alpha_{q'}}$, seems to give a better description of the ageing rate at the first ageing phases. At about 1250 h, $\underline{AD}$, $\underline{N_{PD}(\alpha_{i'})^2}$ and $\underline{N_{PD}\alpha_{q'}}$ increase because the number of PDs per cycle increases drastically from phase D to phase E and the impact energy per PD remains almost constant, see Table I.

IV. Conclusions

The proposed damage function, (8), and method allows evaluating quantitatively the ageing conditions induced by PDs activity in solid dielectrics. The ageing induced by PDs can be related to energy transformations during PDs activity. The chemical mechanism seems to be active along all the ageing phases because the PD impact energy is high enough for activate the chemical reactions. More research is needed for corroborate this. A complete study considering other ageing mechanisms will be presented in a future paper

The impact of PD energy in the cavity can be approximately calculated with (14), considering that the geometry of the cavity is previously known, because the charge carrier dynamics, specifically the drift velocity, is proportional to the peak of PD current. The value of $\underline{N_{PD}(\alpha_{i'})^2}$ along the ageing is indicative of the damage growth rate and can be used with online measurement systems for implementing prognosis tools in conjunction with PRPD and time-resolved measurements. Experimental validation is still required.

Finally, PD charge cannot be taken as a separate diagnostic quantity for evaluating the ageing conditions. The value of the shape factor of the induced PD charge distribution, see Table I, tends to decrease with ageing and can be used as a good ageing indicator.

Acknowledgment

The authors would like to acknowledge Fundación Carolina, Universidad de Antioquia - Departamento de Ingeniería Eléctrica, Universidad Politécnica de Madrid, Fondo Sapiencia - Alcaldía de Medellín and Ministry of Science and Innovation of Spain, National Program of Scientific and Technical Research and Innovation (project PID2019 - 107126RB - C21).

References

[1] M. Chanda and S. K. Roy, Industrial Polymers, Specialty Polymers, and Their Applications, 1st ed. Boca Raton, U.S.A.: CRC Press, 2008.

[2] Y. Shibuya, S. Zoledziowski, and J. H. Calderwood, "Void formation and electrical breakdown in epoxy resin," IEEE Transactions on Power

Apparatus and Systems, vol. 96, no. 1, pp. 198–207, Jan. 1977, doi: 10.1109/T-PAS.1977.32324.

[3] L. A. Dissado and J. C. Fothergill, Electrical Degradation and Breakdown in Polymers, 1st ed. London, U.K.: IET, 1992.

[4] T. Tanaka, "Internal Partial Discharge and Material Degradation," IEEE Transactions on Electrical Insulation, vol. EI-21, no. 6, pp. 899–905, Dec. 1986, doi: 10.1109/TEI.1986.348999.

[5] T. Tanmaneeprasert and P. L. Lewin, "Investigation into accelerated ageing and failure mechanisms of cavities in polyethylene materials using partial discharge techniques," in 2016 International Conference on Condition Monitoring and Diagnosis (CMD), Sep. 2016, pp. 819–823, doi: 10.1109/CMD.2016.7757956.

[6] J. M. Rodríguez-Serna and R. Albarracín-Sánchez, "Numerical Simulation of Temperature and Pressure Changes due to Partial Discharges in Spherical Cavities Within Solid Dielectrics at Different Ageing Conditions," Energies, vol. 12, no. 24, p. 4771, Jan. 2019, doi: 10.3390/en12244771.

[7] G. Mazzanti, G. C. Montanari, and S. Serra, "Aging model of polyethylene-based materials for HV cables founded on damage inception and growth from air-filled voids," in Proceedings of the 2004 IEEE International Conference on Solid Dielectrics, 2004. ICSD 2004., Jul. 2004, vol. 2, pp. 525-529 Vol.2, doi: 10.1109/ICSD.2004.1350484.

[8] G. Mazzanti, G. C. Montanari, and F. Civenni, "Model of Inception and Growth of Damage from Microvoids in Polyethylene-based Materials for HVDC Cables. 1. Theoretical Approach," IEEE Transactions on Dielectrics and Electrical Insulation, vol. 14, no. 5, pp. 1242–1254, Oct. 2007, doi: 10.1109/TDEI.2007.4339485.

[9] G. C. Montanari, "On line partial discharge diagnosis of power cables," in 2009 IEEE Electrical Insulation Conference, May 2009, pp. 210–215, doi: 10.1109/EIC.2009.5166347.

[10] G. C. Montanari and A. Cavallini, "Partial discharge diagnostics: from apparatus monitoring to smart grid assessment," IEEE Electrical Insulation Magazine, vol. 29, no. 3, pp. 8–17, May 2013, doi: 10.1109/MEI.2013.6507409.

[11] M. G. Danikas and G. Adamidis, "Partial discharges in epoxy resin voids and the interpretational possibilities and limitations of Pedersen's model," Electrical Engineering, vol. 80, no. 2, pp. 105–110.

[12] T. Tanmaneeprasert, P. L. Lewin, and G. Callender, "Analysis of degradation mechanisms of silicone insulation containing a spherical cavity using partial discharge detection," in 2017 IEEE Electrical Insulation Conference (EIC), Jun. 2017, pp. 233–236, doi: 10.1109/EIC.2017.8004633.

[13] C. Chang et al., "Developing an experimental method for a cavity PD based life model," in 2013 IEEE International Conference on Solid Dielectrics (ICSD), Jun. 2013, pp. 780–783.

[14] C. Laurent and G. Teyssedre, "Hot electron and partial-discharge induced ageing of polymers," Nuclear Instruments and Methods in Physics Research Section B: Beam Interactions with Materials and Atoms, vol. 208, pp. 442–447, Aug. 2003, doi: 10.1016/S0168-583X(03)00649-9.

[15] J. M. Rodríguez-Serna, R. Albarracín-Sánchez, and I. Carrillo, "An Improved Physical-Stochastic Model for Simulating Electrical Tree Propagation in Solid Polymeric Dielectrics," Polymers, vol. 12, no. 8, Art. no. 8, Aug. 2020, doi: 10.3390/polym12081768.

[16] J. M. Rodríguez-Serna, R. Albarracín-Sánchez, and A. A. Mas'ud, "Finite-element-analysis models for numerical simulation of partial discharges in spherical cavities within solid dielectrics: a review and a novel method," High Volt., vol. 5, no. 5, pp. 556-568, Oct. 2020, doi: 10.1049/hve.2019.0392.

[17] Kuffel E., Zaengl W.S., and Kuffel J., High Voltage Engineering Fundamentals, 2nd ed. Oxford, U.K.: Elsevier, 2000.

[18] F. Gutfleisch and L. Niemeyer, "Measurement and simulation of PD in epoxy voids," IEEE Transactions on Dielectrics and Electrical Insulation, vol. 2, no. 5, pp. 729–743, Oct. 1995, doi: 10.1109/94.469970.

[19] G. C. Montanari, A. Cavallini, L. Testa, S. Serra, and L. A. Dissado, "Model of ageing inception and growth from microvoids in polyethylene-based materials under AC voltage," in 2008 Annual Report Conference on Electrical Insulation and Dielectric Phenomena, Oct. 2008, pp. 29–32.

[20] M. A. Brown, J. V. Champion, S. J. Dodd, and P. Mudge, "An investigation of partial discharge energy dissipation and electrical tree growth in an epoxy resin," in Proceedings of the 2004 IEEE International Conference on Solid Dielectrics, 2004. ICSD 2004., Jul. 2004, vol. 1, pp. 288-291 Vol.1, doi: 10.1109/ICSD.2004.1350347.

[21] J. J. Munro, S. Harrison, M. M. Fujimoto, and J. Tennyson, "A dissociative electron attachment cross-section estimator," Journal of Physics: Conference Series, vol. 388, no. 1, p. 012013, Nov. 2012, doi: 10.1088/1742-6596/388/1/012013.

[22] M. Kurrat, "Energy Consideration for Partial Discharges in Voids," European Trans. on Electr. Power, vol. 2, no. 1, pp. 39–44, Feb. 1992, doi: 10.1002/etep.4450020107.

[23] Woo Seok Kang, Jin Myung Park, Yongho Kim, and Sang Hee Hong, "Numerical study on influences of barrier arrangements on dielectric barrier discharge characteristics," IEEE Transactions on Plasma Science, vol. 31, no. 4, pp. 504–510, Aug. 2003, doi: 10.1109/TPS.2003.815469.

[24] M. Kurrat, "Simulation of Partial-Discharge Processes and Energy Densities," European Trans. on Electr. Power, vol. 5, no. 3, pp. 157–163, Jun. 1995, doi: 10.1002/etep.4450050303.

[25] C. Hudon and R. Bartnikas, "Surface and gas phase reactions arising with epoxy exposed to partial discharges," in [Proceedings] 1992 Annual Report: Conference on Electrical Insulation and Dielectric Phenomena, Oct. 1992, pp. 725–734, doi: 10.1109/CEIDP.1992.283133.

[26] M. Mozetič, A. Vesel, G. Primc, and R. Zaplotnik, "Chapter 2 - Introduction to Plasma and Plasma Diagnostics," in Non-Thermal Plasma Technology for Polymeric Materials, S. Thomas, M. Mozetič, U. Cvelbar, P. Špatenka, and P. K.m., Eds. Elsevier, 2019, pp. 23–65.

[27] J. T. Holboll and M. Henriksen, "Partial discharge patterns related to surface deterioration in voids in epoxy," in IEEE International Symposium on Electrical Insulation, Jun. 1990, pp. 115–119, doi: 10.1109/ELINSL.1990.109721.

[28] R. Schurch, S. M. Rowland, and R. S. Bradley, "Partial discharge energy and electrical tree volume degraded in epoxy resin," in 2015 IEEE Conference on Electrical Insulation and Dielectric Phenomena (CEIDP), Ann Arbor, USA, Oct. 2015, pp. 820–823, doi: 10.1109/CEIDP.2015.7352053.

[29] N. Hozumi and T. Okamoto, "The initiation and growth of AC tree in polyethylene," in 3rd International Conference on Conduction and Breakdown in Solid Dielectrics, Trondheim, Norway, Jul. 1989, pp. 543–547, doi: 10.1109/ICSD.1989.69256.

[30] M. Borghei, M. Ghassemi, J. M. Rodriguez-Serna, and R. Albarracin, "A Finite-Element-Analysis and an Improved Induced Charge Concept for Partial Discharge Modeling," IEEE Transactions on Power Delivery, accepted, 2020, doi: 10.1109/TPWRD.2020.2991589.

[31] A. Pedersen, "Partial discharges in voids in solid dielectrics. An alternative approach," in Conference on Electrical Insulation Dielectric Phenomena — Annual Report 1987, Oct. 1987, pp. 58–64, doi: 10.1109/CEIDP.1987.7736534.

[32] J. Lawless, Statistical Models and Methods for Lifetime Data, 2nd ed. New Jersey, USA: Wiley, 2011.

[33] M. D. L. del Casale and R. Schifani, "Investigation of temperature effect on an epoxy resin: Aging due to partial discharges," in 2000 Eighth International Conference on Dielectric Materials, Measurements and Applications, Sep. 2000, pp. 509–512, doi: 10.1049/cp:20000561.

[34] G. C. Montanari, P. Morshuis, P. Seri, and R. Ghosh, "Ageing and reliability of electrical insulation: the risk of hybrid AC/DC grids," High Volt., vol. 5, no. 5, pp. 620–627, Apr. 2020, doi: 10.1049/hve.2019.0371.

[35] K. Uchida, H. Asai, N. Shimizu, and T. Takahashi, "Initiation mechanism of electrical tree and deteriorated region in polymers," in Proceedings of the 3rd International Conference on Properties and Applications of Dielectric Materials, Jul. 1991, pp. 240–243 vol.1, doi: 10.1109/ICPADM.1991.172018.

[36] K. Temmen, "Evaluation of surface changes in flat cavities due to ageing by means of phase-angle resolved partial discharge measurement," J. Phys. D: Appl. Phys., vol. 33, no. 6, pp. 603–608, Mar. 2000, doi: 10.1088/0022-3727/33/6/303.

[37] L. Wang, A. Cavallini, G. C. Montanari, and L. Testa, "Evolution of pd patterns in polyethylene insulation cavities under AC voltage," IEEE Transactions on Dielectrics and Electrical Insulation, vol. 19, no. 2, pp. 533–542, Apr. 2012, doi: 10.1109/TDEI.2012.6180247.

Anexo D: resumen de publicaciones y productos de investigación

En este anexo se presenta un resumen de las publicaciones y otros productos de investigación realizados durante los estudios de doctorado. En la siguiente tabla se resumen las publicaciones, se incluyen el título de las publicaciones y los autores e información general de las revistas o eventos, tales como el año, si es o no de acceso abierto, la clasificación en JCR y Scopus, el número de citas, el DOI y el ISSN o ISBN.

Tabla 27. Resumen de publicaciones realizadas durante los estudios de doctorado.

	Título	Autores	Revista /Evento	Acceso abierto	Año	Clasificación		Citas	ISSN/ ISBN	DOI
						JCR	Scopus			
1	Modeling Oil-paper Insulation Frequency-Domain Spectroscopy Based on its Microscopic Dielectric Processes	Jiacheng Xie, Ming Dong, Yizhuo Hu, Tianxin Zhuang, Ricardo Albarracín-Sánchez y Johnatan M. Rodríguez-Serna	IEEE Transactions on Dielectrics and Electrical Insulation	No	2019	Q2	Q2	4	1558-4135	10.1109/TDEI.2019.008155
2	Numerical simulation of temperature and pressure changes due to partial discharges in spherical cavities within solid dielectrics at different ageing conditions	Johnatan M. Rodríguez-Serna y Ricardo Albarracín-Sánchez	Energies	Sí	2019	Q3	Q2	5	1996-1073	10.3390/en12244771
3	Separation of partial discharges sources measured in the high-frequency range with HFCT sensors using a 3D-Phased-Resolved pattern	Ricardo Albarracín-Sánchez, Fernando Álvarez-Gómez, Carlos A. Vera-Romero y Johnatan M. Rodríguez-Serna	Sensors	Sí	2020	Q1	Q1	9	1424-8220	10.3390/s20020382
4	Finite-Element-Analysis Models for Numerical Simulation of Partial Discharges in Spherical Cavities within Solid Dielectrics: A Review and a Novel Method	Johnatan M. Rodríguez-Serna, Ricardo Albarracín-Sánchez y Abdullahi A. Mas'ud	High Voltage	Sí	2020	Q2	Q1	5	2397-7264	10.1049/hve.2019.0392
5	Computer Simulation of Partial Discharges in Voids inside Epoxy Resins Using Three Capacitance and Analytical Models	Johnatan M. Rodríguez-Serna, Ricardo Albarracín-Sánchez, Ming Dong y Ming Ren	Polymers	Sí	2020	Q1	Q1	4	2073-4360	10.3390/polym12010077
6	A Finite-Element-Analysis and an Improved Induced Charge Concept for Partial Discharge Modeling	Moein Borghei, Mona Ghassemi, Johnatan M. Rodríguez-Serna y Ricardo Albarracín-Sánchez	IEEE Transactions on Power Delivery	No	2020	Q1	Q1	12	0885-8977	10.1109/TPWRD.2020.2991589
7	An Improved Physical-Stochastic Model for Simulating Electrical Tree Propagation in Solid Polymeric Dielectrics	Johnatan M. Rodríguez-Serna, Ricardo Albarracín-Sánchez e Isabel Carrillo	Polymers	Sí	2020	Q1	Q1	3	2073-4360	10.3390/polym12081768

8	Improved Deterministic and Stochastic Models for Simulating Partial Discharges in Non-Conducting Trees Inside Solid Dielectrics	Johnatan M. Rodríguez-Serna y Ricardo Albarracín-Sánchez	High Voltage	Sí	2020	Q2	Q1	1	2397-7264	10.1049/hve2.12038
9	A Study on the Life Estimation and Cavity Surface Degradation Due to Partial Discharges in Spherical Cavities within Solid Polymeric Dielectrics Using a Simulation Based Approach	Johnatan M. Rodríguez-Serna y Ricardo Albarracín-Sánchez	Polymers	Sí	2021	Q1	Q1	0	2073-4360	10.3390/polym13030324
10	Partial Discharges Measurements for Condition Monitoring and Diagnosis of Power Transformers: A Review	Johnatan M. Rodríguez-Serna, Ricardo Albarracín-Sánchez, Fernando Garnacho, Fernando Álvarez y Javier Ortego	Advanced Research Workshop on Transformers - ARWtr2019	No	2019	-	-	5	978-84-09-11743-7	10.23919/ARWtr.2019.8930183
11	Streamer Simulation in Nanodielectric Fluids at Different Fe_3O_4 nanoparticle Concentrations	Johnatan M. Rodríguez-Serna, Ricardo Albarracín-Sánchez, Juan Velasco, Ricardo Frascella y Victor A. Primo	2019 IEEE 20th International Conference on Dielectric Liquids (ICDL)	No	2019	-	-	1	978-1-7281-1718-8	10.1109/ICDL.2019.8796558
12	Simulation of Polymeric Insulators Ageing Induced by the Impact Energy of Electrons During Partial Discharge Activity	Johnatan M. Rodríguez-Serna y Ricardo Albarracín-Sánchez	2021 IEEE Texas Power and Energy Conference	No	2021	-	-	0	978-1-7281-8612-2	10.1109/TPEC51183.2021.9384986

De la Tabla 27, se puede concluir que el 77,80 % de las publicaciones de revistas fueron publicadas en revistas del primer cuartil (Q1) en la clasificación Scopus mientras que 22,20 % en revistas del segundo cuartil (Q2) de la misma clasificación. De manera similar, pero considerando la clasificación JCR, el 55,55 % de los artículos de revista están en revistas del primer cuartil (Q1), 33,33 % en revistas del segundo cuartil (Q2) y 11,11 % en revistas del tercer cuartil (Q3). De las 12 publicaciones realizadas, tres corresponden a artículos de conferencia en eventos organizados por asociaciones pertenecientes al *Institute of Electrical and Electronics Engineers* – IEEE, por lo que los artículos se incluyen en las bases de datos de IEEE Xplore (https://ieeexplore.ieee.org/Xplore/home.jsp). De manera gráfica, la siguiente figura muestra las publicaciones realizadas durante los tres años de doctorado junto con las citas recibidas hasta la fecha del 26 de mayo de 2021.

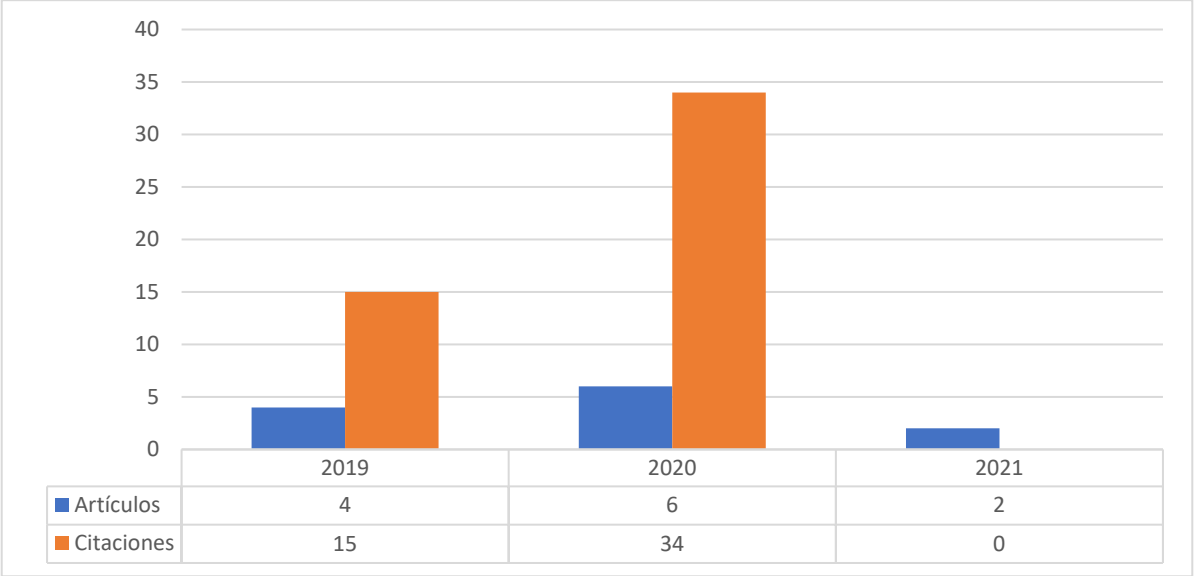

Figura 28. Distribución de las publicaciones realizadas durante los tres años de doctorado con citas recibidas.

Hasta la fecha anteriormente mencionada, las publicaciones han recibido un total de 49 citaciones. Adicionalmente, se han podido obtener los siguientes productos de investigación:

Registro de software:

- Aplicación (app) de MATLAB® llamada PDSym-1S, que permite la simulación de DP en cavidades esféricas. Esta aplicación fue registrada ante la OTRI de la UPM

Asesoría a estudiantes en trabajos de fin de grado:

- Trabajo de fin de grado titulado "Simulación de propagación de arborescencias en sistemas de aislamiento eléctrico", realizado por el estudiante Marco Antonio Narvaez Romero, en el año 2020
- Trabajo de fin de grado titulado "Procesamiento y análisis de señales con la herramienta Signal Processing de MATLAB®", realizado por el estudiante Zhicheng Jiang, en el año 2020

Asesoría estudiantes programa de excelencia México:

- Tres estudiantes, proyectos relacionados con programación en MATLAB®, simulación de DP y desarrollo de un aplicativo en MATLAB® (app) para la separación de fuentes de DP llamado PRPD-time

Participación en proyectos:

- Proyecto "Gestión del ciclo de vida de transformadores aislados con fluidos biodegradables", Agencia Estatal de Investigación (proyecto PID2019-107126RB-C21)
- Proyecto "Research and testing of new EMC systems based on multiprobe setups", Microwave Vision Italy

LISTA DE FIGURAS

LISTA DE TABLAS